Marine Geology 407 (2019) 76–93

Contents lists available at ScienceDirect

Marine Geology

journal homepage: www.elsevier.com/locate/margo

Post-spreading deformation and associated magmatism along the Iberia-Morocco Atlantic margins: Insight from submarine volcanoes of the Tore-Madeira Rise

Guillaume Sanchez[a,*], Renaud Merle[b], Florent Hinschberger[c], Isabelle Thinon[d], Jacques Girardeau[e]

[a] *Frogtech Geoscience, Suite 17F, Level 1, 2 King Street, Deakin West, ACT 2600, Australia*
[b] *Swedish Museum of Natural History, S-104 05, Stockholm, Sweden*
[c] *EA 6293 GéHCO-Université de Tours - UFR Sciences et Techniques, Parc de Grandmont, 37200 Tours, France*
[d] *French Geological survey-BRGM, 3 avenue Claude-Guillemin BP 36009, 45060 Orléans Cedex 2, France*
[e] *Laboratoire de Planétologie et Géodynamique, UMR-CNRS 6112, Université de Nantes, 2 rue de la Housssinère, 44322 Nantes Cedex 3, France*

ARTICLE INFO

Editor: Michele Rebesco

Keywords:
Volcanism
Oceanic transform
Transfer faults
Transtension
Tore-Madeira Rise
Iberia-Morocco margin

ABSTRACT

A new high-resolution bathymetric map combined with a regional Digital Elevation Model (DEM) analysis reveal the modalities of occurrence and emplacement of post-spreading magmatism along the NNE-SSW oriented, 1000 km long Tore-Madeira Rise (TMR) as well as its relationship with the activity of major fault systems including the Estremadura Fault System (ESF) and the Azores-Gibraltar Fracture Zone (AGFZ). Morphological and structural analysis of the bathymetric map were performed to map volcanic features such as eruptive cones, vents and fissures together with faults along the TMR. The new bathymetric map shows that the main NNW-SSE seamount alignment is formed by three structurally distinct volcanic massifs, the Tore, the Josephine and the Southern Volcanic Groups. The majority of the volcanoes of each group emplaced within or along specific portion of pre-existing faults (ESF and AGFZ) including splay fault, releasing bend, fault tips and interaction zones between different segments. Magmas were channelled into sub-vertical pre-existing lithospheric faults that acted as preferential pathways for the vertical magma ascent. Migration and final eruption of magma are controlled by the local stress variation induced by complex fault geometries, change in plate kinematics as well as strong shear zone anisotropy as suggested by the emplacement within localised areas of transtension. We conclude that post-spreading magma emplacement in the southern part of the Iberia margin was related to the development of a transtensional plate boundary between the Iberian and African Plate during the Late Cretaceous. More generally, our findings emphasize that the distribution of volcanism as the expression of the interaction between shallow plate tectonic and mantle processes should be included in plate kinematic reconstruction. This study also demonstrates that the accurate mapping of oceanic seafloor is pivotal to better understand tectono-magmatic evolution of volcanic seamount chains and geological processes in oceanic domains.

1. Introduction

In oceanic basins in the vicinity of continents, extensive intraplate volcanism emplaces after oceanic spreading within pre-existing crust that undergone multiple phase of deformation. Hence, lithospheric discontinuities are likely able to control the spatial distribution of intraplate volcanism and possibly its timing. However, the role of the plate architecture and the influence of lithospheric structures on magma ascent and localisation of volcanic eruptions in oceanic basins still remain unclear (e.g. Natland and Winterer, 2005). Plate extension, lithospheric cracking resulted in the development of either linear, sometimes age-progressive volcanic trails or scattered, polygenic and polyphased magmatism along pre-existing or potentially new fractures that have been reported in many oceanic basins (Davis et al., 2002; O'Connor and Jokat, 2015; Song et al., 2017). On the other hand, several studies also argue that magma may enhance localisation of strain and influence plate boundaries (Calais et al., 2008; Trippanera et al., 2014).

* Corresponding author.
E-mail address: gsanchez@frogtech.com.au (G. Sanchez).

https://doi.org/10.1016/j.margeo.2018.10.011
Received 7 June 2018; Received in revised form 12 October 2018; Accepted 25 October 2018
Available online 01 November 2018

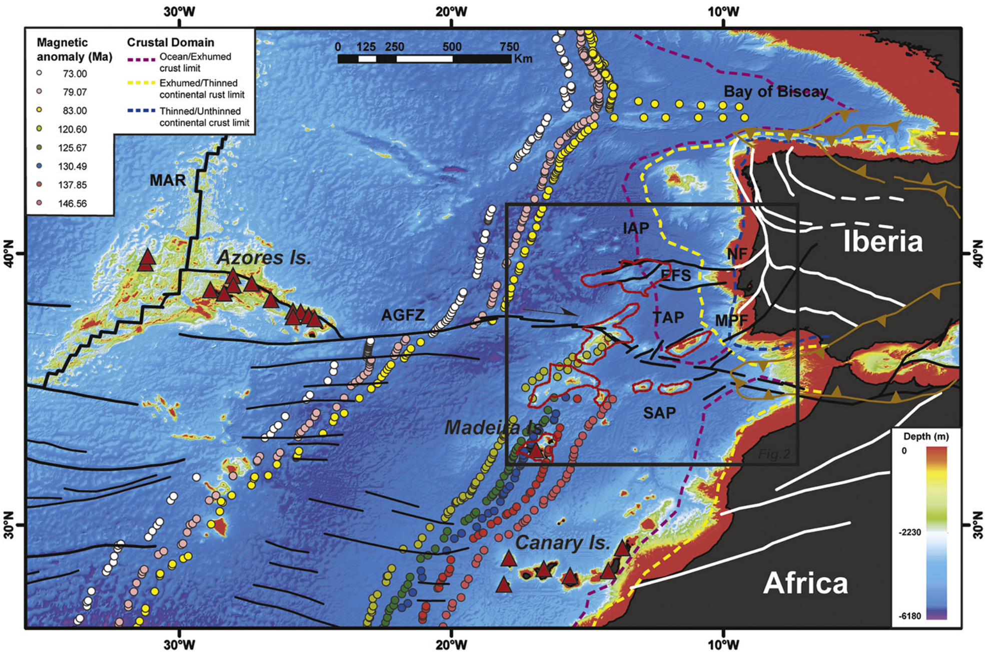

Fig. 1. Bathymetric maps of the Iberia-Morocco margin within the southern North Atlantic and northern Central Atlantic showing the recent to present-day configuration of the plate boundary between the Iberia and NW Africa plates. Red dashed lines represent the Tore-Madeira Rise volcanic fields. AGFZ: Azores-Gibraltar Fracture Zone, IAP: Iberia Abyssal Plain, TAP: Tagus Abyssal Plain, SAP: Seine Abyssal Plain, MAR: Mid-Atlantic Ridge. MPF: Messejana-Plasencia Fault; NF: Nazaré Fault. Active volcanoes are represented in red triangles. Coloured dots: Magnetic anomalies extracted from Seton et al. (2014). Thick white lines: major fractures zone from Matthews et al. (2011). White lines represent major inherited structures from the Late Cretaceous (modified from Alves and Abreu Cunha, 2018 and Ballevre et al., 2014). Crustal rift domain boundaries modified from Afilhado et al. (2008); Nirrengarten et al. (2017); Pereira et al. (2016); Ramos et al. (2017); Sallarès et al. (2013). Location of Fig. 2 is represented by the black rectangle. Projection latitude/longitude coordinates according to the WGS84 system. (For interpretation of the references to colour in this figure legend, the reader is referred to the web version of this article.)

The Tore-Madeira Rise (TMR), a roughly NNE-SSW trending seamounts chain (Fig. 1), represents one of the most significant magmatic features that emplaced along the Iberia-Morocco margin in the northern central Atlantic Ocean from the Late Cretaceous to recent times (Merle et al., 2009, 2018). The Early Mesozoic continental rifting affecting the Pangea supercontinent resulted in margin segmentation, formation of transfer faults and new basement at distal margin. Such lithospheric heterogeneities are likely to control magma pathways and volcanic eruptions by several factors including rock anisotropy, fault geometry, differential stress and thermal regime (e.g. Tibaldi, 2015). Although many authors have suggested the involvement of the lithospheric discontinuities to explain the location of the magmatic occurrences on TMR (Geldmacher et al., 2006; Merle et al., 2006), the morphology of TMR seamounts together with fault geometry were never investigated despite this might provide key evidences on the origin and formation of TMR.

The determination of tectonic models and our understanding of tectono-magmatic processes are critically dependent on accurate mapping of the ocean-floor structures. Global DEM datasets with an increasing accuracy and spatial resolution are now publicly available which allows better quantitative surface analysis at the regional-scale. However, morphology of volcanoes, eruptive fissures and faults geometry can only be detected with higher resolution data (e.g. 20–100 m spatial resolution). The new TOREMADERE bathymetry data were, thus, acquired to give a higher-resolution image of the seafloor structures. This paper presents the first detailed map of the topography and major morpho-tectonic structures of the TMR seamounts with the aim of deciphering the structural control on TMR formation and bring new constrains on its origin as well as on post-spreading deformation of the Iberia-Morocco.

2. Geological setting

2.1. The western Iberia and north-west Morocco margin

The West Iberia and the NW Morocco margins belong respectively to the northern Central Atlantic and southern North Atlantic Oceans which are separated by the Azores-Gibraltar Fracture Zone (AGFZ; Fig. 1). These margins formed during several phases of continental rifting affecting Pangea from the Late Triassic until the Late Cretaceous (e.g. Tucholke et al., 2007; Péron-Pinvidic and Manatschal, 2009; Schettino and Turco, 2009; Frizon De Lamotte et al., 2015). Rifting events culminated in final continental break-up, mantle exhumation, initiation of oceanic seafloor spreading and subsequently to the separation of the Iberia, NW Africa and North America plates (Fig. 1) from the Late Jurassic-Early Cretaceous (Féraud et al., 1988; Boillot et al., 1989; Srivastava et al., 2000; Sahabi et al., 2004; Tucholke et al., 2007; Schettino and Turco, 2009; Bronner et al., 2011; Kneller et al., 2012; Nirrengarten et al., 2018).

Despite mantle exhumation is constrained around 143–122 Ma (e.g. Féraud et al., 1988; Schärer et al., 2000), formation of the first oceanic crust in this area is highly debated possibly between 125 and 112 Ma, depending on the J- magnetic anomaly interpretation (Fig. 2). Although successively interpreted as related to an oceanic magnetic anomaly (Srivastava et al., 2000), or to the transition between exhumed mantle and oceanic crust (Bronner et al., 2011), the origin of the J magnetic anomaly has been recently attributed to a thickened crust or basement high related to *syn-* and post-spreading (i.e. TMR) magmatic underplating (Bronner et al., 2011; Nirrengarten et al., 2017). The southern continuation of the J magnetic anomaly, south of the AGFZ corresponds, however, to the M0 isochron of the mid-Atlantic ridge (Klitgord and Schouten, 1986).

Mid-ocean ridge activity started during the Late Jurassic-Early Cretaceous along the SW Iberia margin and migrated northward with the final break-up on the NW Iberia-Newfoundland margin at Albian-Aptian time (Fig. 2; Tucholke et al., 2007; Bronner et al., 2011; Nirrengarten et al., 2018;). Spreading was directed NE-SW during the Late Jurassic-Early Cretaceous and change direction toward an E-W axis in relation to the clockwise rotation of Iberia and the opening of the central segment of the North Atlantic (e.g. Vissers and Meijer, 2012; Barnett-Moore et al., 2016; Nirrengarten et al., 2018). In the meantime, left-lateral oblique plate motion along the South Iberia margin resulted in segmented oceanic spreading during the Late Jurassic connecting the Atlantic Ocean (i.e. AGFZ; Féraud et al., 1977) to the Alpine Tethys (Martínez-Loriente et al., 2014; Ramos et al., 2017; Sallarès et al., 2011, 2013).

During the three main periods of rifting from the Late Triassic to the late Early Cretaceous, basin geometry was controlled by major E-W and

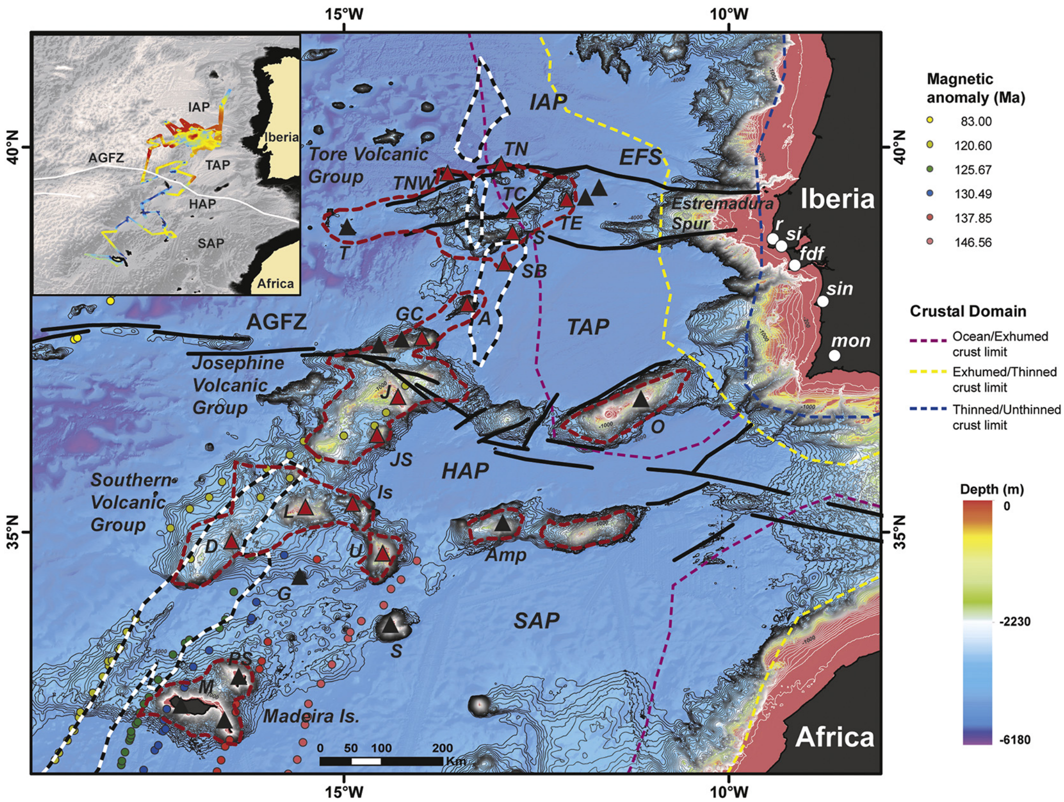

Fig. 2. Bathymetric map of the Tore-Madeire Rise from the compiled EMODnet bathymetric grid including the Toremadere HR bathymetric data and satellite derived GEBCO data. These map shows the main volcanic edifices (red triangles) of the Tore-Madeira Rise and surroundings seamounts (Black triangles). Amp: Ampere, A: Asthon, D: Dragon, FdF: Foz da Fonte, G: Godzilla, GC: Gago Coutinho, Is: Isabelle, J: Josephine, JS: Jo Sister, M: Madeira, Mon: Serra de Monchique, O: Ormonde, PS: Porto Santo, R: Ribamar, S: Seine, Sin: Sintra, Si: Sines, SB: Sponge Bob, T: Torillon, TC: Tore Central, TE: Tore East, TN: Tore North, TNW: Tore North-West, TS: Tore South, U: Unicorn. White-black dashed line: location of the positive J- magnetic anomaly (Bronner et al., 2011; Nirrengarten et al., 2017). Bathymetric contours (200 m) are derived from the EMODnet DEM described in this study. Box: Position of the TOREMADERE HR multibeam bathymetric survey (coloured) on the EMODNet bathymetric map. For references on magnetic anomaly, crustal domain boundaries and inherited faults, see Fig. 1. (For interpretation of the references to colour in this figure legend, the reader is referred to the web version of this article.)

NE-SW transfer faults including the Nazaré Fault Zone and the Messejana-Plasencia Fault Zone (Fig. 1) which correspond to pre-existing crustal structures formed during the Late Variscan Orogeny (Pereira and Alves, 2012; Ramos et al., 2017). Rift migration resulted in along-axis crustal segmentation and development of several sub-basins bounded by NNW-SSE to N-S major faults with distinct tectonic and subsidence evolution along the West Iberia margin (Alves et al., 2009; Pereira and Alves, 2011; Fig. 1). During the Cenozoic to present-day, the Iberia margin experienced widespread inversion due to the northward convergence of Africa (Vergés et al., 2002). Although well defined in the proximal domain of the margin (i.e. the Estremadura Fault System: EFS; Fig. 1; Fig. 2), the western continuity of these faults at the transition between the distal continental and oceanic domains are, however, less clear due to recent reactivation along these structures (Pereira et al., 2016).

2.2. The TMR and surrounding seamounts

TMR is defined as a NNE-SSW aligned seamounts chain, located along the margins of Portugal and Morocco and straddling the AGFZ without visible offset (Fig. 2). It extends over 1000 km, between the Tore seamounts and Madeira Archipelago, which forms the southernmost complex of the TMR. The main trend is formed by, from north to south, Tore Volcanic Field, Sponge Bob (SB), Ashton (A), Gago Coutinho (GC), Josephine (J), Jo Sister (JS), Lion (L), Dragon (D) and Godzilla (G, Fig. 2). The westernmost seamount of the Tore Volcanic Field is Torillon lying at around 100 km on the WSW of Tore. Note that a group of three seamounts (Isabelle, Unicorn and Seine) is located slightly on the east of the main alignment. This general NNE-SSW trend is parallel to the high amplitude curvilinear J-magnetic anomaly extending from the Galicia margin to the Madeira archipelago (Fig. 2).

The magmatism on TMR is dated between 103 Ma to 0.5 Ma (Geldmacher et al., 2000, 2006; Merle et al., 2006, 2009, 2018) represented by Oceanic Island Basalt (OIB)-like alkaline lavas ranging in term of petrological types from basalts to trachytes. The TMR magmatism has been interpreted as (1) the first activity of the mid-Atlantic ridge (Tucholke and Ludwig, 1982; Peirce and Barton, 1991); (2) an accretion-related off-axis magmatic activity (Jagoutz et al., 2007); (3) the 450 km-wide Madeira hot-spot track imprint on the Iberia plate that is based on the apparent decreasing age along a track spanning from Serra de Monchique to Madeira archipelago through Seine, Unicorn, Ampere and Ormonde (Geldmacher et al., 2000, 2001; D'Oriano et al., 2010); (4) the result of the combined effects of the Canary hot-spot during Cretaceous times forming the basement of the rise which was capped by late Tertiary to recent volcanics related to the Madeira hot-spot (Geldmacher et al., 2000, 2006; D'Oriano et al., 2010); or (5) a large thermal anomaly located beneath the lithosphere and emitting magma pulses, the geographical and timing of the magmatic occurrences being the consequence of the interaction between these magma pulses and the complex motions of the Iberia plate controlled by the Pyrenees Orogeny (Merle et al., 2009, 2018).

Table 1
Summary of the main morphology characteristics of the TMR volcanoes. Ages of volcanic edifices are quoted from Féraud et al. (1981, 1982, 1986), Bernard-Griffiths et al. (1997), D'Oriano et al. (2010), Geldmacher et al. (2000, 2005, 2006, 2008), Grange et al. (2010), Merle et al. (2006, 2009) and Miranda et al. (2009). See text for details.

TMR Volcanoes (N to S)		Summit elevation (m msl)	Seafloor depth (m msl)	Seamount height (m)	Major-axis length (Lma - km)	Minor-axis length (Lma-km)	Ellipticity (Lma/Lma)	Age (Ma)
Tore NW	*TNW*	−2600	−5300	2700	35.70	22.60	0.63	80
Tore N - west	*TN*	−2800	−5300	2500	34.38	23.39	0.68	–
Tore N - east	*TN*	−3200	−5100	1900	27.22	18.94	0.70	88
Tore E - VE1	*TE*	−2500	−3900	1400	13.60	9.80	0.72	88
Tore E - VE2		−3600	−4700	1100	11.70	9.99	0.85	–
Tore E - VE3		−3600	−4600	1000	17.80	10.30	0.58	–
Tore E - VE4		−3900	−4900	1000	11.04	9.03	0.82	–
Tore C	*TC*	−3400	−5000	1600	11.49	5.50	0.48	–
Sponge Bob	*SB*	−3200	−4600	1400	19.46	10.88	0.56	103
Asthon	*A*	−1500	−3800	2300	24.88	21.43	0.86	99–96
Asthon Ridge	*AR*	−3500	−4300	800	13.50	4.48	0.33	–
Gago-Coutinho	*GC1*	−1300	−4600	3300	38.44	28.09	0.73	96–92
Gago-Coutinho	*GC2*	−1400	−3600	2200	24.73	17.68	0.71	–
Gago-Coutinho	*GC3*	−1400	−4100	2700	8.10	4.62	0.57	–
Josephine	*J*	−300	−4000	3700	65.80	21.87	0.33	16–12 8–0.5
Josephine - VE1		−800	−1700	900	16.28	10.15	0.62	–
Josephine - VE2		−800	−2500	1700	23.02	16.73	0.73	–
Jo Sister	*JS*	−1000	−3300	2300	26.84	20.44	0.76	88–86.5
Lion	*L*	−600	−2800	2200	65.53	16.97	0.26	–
Isabelle	*Is*	−1800	−4200	2400	53.61	28.49	0.53	> 85
Unicorn	*U*	−800	−4200	3400	70.30	26.63	0.38	28
Dragon	*D*	−1300	−2600	1300	40.24	18.93	0.47	1.0–4.0

3. Data and methods

3.1. Database

Between September and October 2001, a total of 95000 km^2 of High Resolution (HR) swath bathymetry were acquired during the TOREMADERE survey (see details on http://dx.doi.org/10.17600/1010110) aboard the Atalante R/O vessel, using a SIMRAD DUAL EM12 swath Multibeam Echo sounder system. This survey provided a high-resolution bathymetry map of the Tore Seamount Complex and several seamounts of the TMR which were identified as volcanic edifices (Fig. 2). The vertical resolution of the SIMRAD instrument is estimated at approximately 10–20 m with a maximum of 50 m at 4000–5000 m depth representing an error of 1%. Raw data from the survey were first processed using the GENAVIR on-board processing software to perform geometric correction due to refracted sound waves. The processed data were exported as an ASCII XYZ point file. Bathymetry was then converted into a 100 m spatial resolution grid by nearest-neighbour interpolation and imported into QGIS3.0 for spatial analyses.

The latest EMODnet bathymetry (Marine Information Service, 2016) for the studied area was downloaded from the EMODnet Bathymetry portal (http://www.emodnet-bathymetry.eu). This EMODnet grid combines a number of different data sources such as High-Resolution single and multiple beam bathymetric surveys including the bathymetric survey of the TOREMADERE cruise as well as composite DTMs produced by external providers (e.g. International Hydrographic Organisation). To obtain a complete coverage of the area, gaps and voids were filled by the GEBCO 2014 30″ gridded data (Fig. 2). The EMODnet bathymetric grid has a pixel size of 1/8-min arc (for further details and explanation on gridding procedures, we refer to the EMODnet portal). Features mapped have a minimum spatial resolution of ~230 m at the latitude of the area of interest. Elevation contour lines were generated with the elevation interval chosen depending on the DEM resolution. The interval should be approximately half the pixel size (e.g., a ~100 m contour interval for the 230 m spatial resolution EMODnet DTM).

3.2. Volcanic edifice morphology and structural analyses

To better understand the structural control on the morphology of volcanoes along the TMR as well as its relationship with magma pathways in its ascent, we analysed volcanic alignment combining with mapping of faults. First, we quantified the morphometric parameters of volcanic edifices, vents and eruptive fissures as well as lineaments on the HR TOREMADERE bathymetry and derived slope distribution maps. Eruptive fissures have been identified or inferred from the alignment of closely spaced vents, breaching direction or crater elongation if preserved (Tibaldi, 1995; Fig. 4). We assume that vents alignments form relatively straight lines along fissures and vents are subparallel to the overall trace alignment and the subsurface feeder dykes (Tibaldi, 1995). The EMODnet bathymetric grid was then used to characterise the geometry of the volcanic and tectonic structures at a regional-scale. Given that the spatial resolution of the EMODnet grid is approximately 230 m, we selected the features that have a horizontal length equal or superior to ~250 m which is below the documented average spacing between vents following Applegate (2003) recommendations.

Volcanic vents were identified from bathymetric maps either raster images or contour intervals each of which has intrinsic limitations. Indeed, ambiguity and in turn uncertainties exist in the identification of such features in areas affected by destruction processes such as submarine landslides. Similar contour geometries can be related to either gravitational processes or represent the location of a vent. We thus mapped volcanic vents that are morphologically recognisable. The alignments of three or more vents forming part of the same volcanic edifice or one volcanic cone characterised by an elliptical shape were used to identify eruptive fissures. All these morphological information of each studied volcano were obtained using QGIS3.0 and are summarised in Table 1 including a reference list for the age of the volcanoes. Stereograms of eruptive fissures and faults were drawn for each area.

4. Description of TMR submarine volcanoes morphology and structure

The EMODnet bathymetric map (Fig. 2) shows clearly that TMR seamounts can be grouped into three massifs: the northernmost Tore

Seamounts Group, the Joséphine Seamount Group in the central part in the vicinity of the AGFZ and the Southern Seamount Group. In addition, the HR bathymetric data highlight for the first-time typical morphological features of volcanic edifices such as elongated cone-shaped edifices, linear ridges, large massifs, isolated cones, eruptive fissures and lava flows along the TMR (Fig. 2). This confirms that most of the reliefs making up the TMR formed as a result of volcanic effusive activity. The rocks dredged during the TOREMADERE cruise were lavas including mostly basalts, south of the AGFZ and trachyandesites and trachytes, north of the AGFZ (Geldmacher et al., 2006; Merle et al., 2005, 2006, 2009). The maximum depth of the seafloor along the TMR ranges between 3500 m and 5000 m. All the mapped seamounts have a height ranging between 2000 and 4000 m above the surrounding seafloor (Table. 1). Summits of some of the volcanoes belonging to the Tore Seamounts Group are at around 2500 m above the seafloor while the highest seamounts along the TMR such as the Joséphine, Lion and Unicorn seamounts are 3500 m high and lie between 300 m and 800 m below sea level. The largest of these seamounts have a base diameter of ~20 to ~50 km (Tore NW, Ashton, Gago Coutinho: 20–30 km, 48 km for Seine). Such dimensions are comparable to the largest continental volcanoes (Mount Etna: 47 × 38 km, 3350 m above sea level). Sponge Bob and Tore East seamounts are smaller with a base diameter of ~10 km.

4.1. Submarine volcanoes of the Tore Seamounts group

The Tore Seamounts Group, the largest volcanic complex of the TMR occurs at the northern end of TMR, to the west of the Estremadura Spur and the West Iberian margin (Fig. 2). HR swath bathymetric map (Fig. 3) reveals a highly complex tore-like shape morphology including several prominent topographic features (Fig. 3a) such as:

(i) a deep basin (Tore Depression) which lies in the central part of the area surrounded by uplifted plateaus (Tore Plateaus) located at an average depth of ~3000 m. This depression displays asymmetric rhombohedra shape oriented N*E*-SW with a maximum depth of the seafloor of 5500 m to the NE;

(ii) several E-W to NNE-SSW elongated topographic highs that rise above the seafloor and are unambiguously interpreted as submarine volcanoes.

The Tore North (Tore N) and Tore North-West (Tore NW) volcanoes located at the northern edge of the Tore Volcanic Group area at the transition with the IAP (Fig. 2) correspond to E-W elongated volcanic seamounts composed of a main volcanic edifice connected to a NE-SW oriented ridge (Table 1; Fig. 3; Fig. 4a,b). The Tore N displays an ~E-W trending rift zone with a main broad rectangular-shaped cone on the south-western part of the edifice. The linear, ENE-WSW-trending, flat-topped ridge linked up the western flank of the main edifice to the second edifice to the east. Flanks on the northern side have average slope values up to 25–30° (Fig. 3b). The southern flank is narrower, characterised by steep slopes that exceed 40° and scarps (Fig. 3b). Tore NW also displays an overall *E*-W trending rift zone with the main cone located on the western part of the volcano (Fig. 4b). The smaller edifice was constructed as an attachment to the eastern flank of the main cone. Tore NW shows series of linear, narrow and deep gullies radiating from the main cone summit (i.e. U-shaped slope channel on Fig. 4b). Small scale hummocks on the seafloor surrounding the south-western side of the volcano are interpreted as debris from landslide. To note, embayments along with over steepened slopes on both Tore N and Tore NW suggest that the flanks of both volcanoes have experienced intense slope failure processes.

To the east of the Tore depression, several smaller volcanic edifices form the eastern part of the volcanic field (Fig. 3a). The Tore East (Tore E) volcano representing the largest edifice presents a N*E*-SW oriented sub-elliptical conical shape with the main cone located on its southern flank (Table 1; Fig. 3a; Fig. 4c). The northern flank of the volcano shows distinct morphology related to lava terraces with flat or gently dipping slopes. The Tore Central edifice is located on the southern edge of the Tore Depression (Fig. 3). It consists of several NE-SW to NNW-SSE linear volcanic ridges (Fig. 4e) while the Tore South edifice presents an E-W elongated edifice that turns to a NNE-SSW en-echelon ridge (Fig. 4f). South of the Tore Volcanic Group in the TAP, a small elliptical edifice, the Sponge Bob volcano presents a broad symmetrical shape along the WNW-ESE axis with an elongated plateau localised at 800 m above the seafloor on its SE flank (Table 1, Fig. 4d).

> 250 eruptive vents were identified across the Tore Volcanic Group area (Fig. 4) from HR bathymetric map. Most of the vents are located in the central domain of the volcano as part of the Rift Volcanic zone. A total of 120 eruptive fissures were mapped with predominantly three strike families: N10–20°E, N80–90°E and N120–130°E (Fig. 11a).

4.2. Central group: Josephine Volcanic Group

The Josephine Volcanic Group is located at the vicinity of the AGFZ (Fig.2), forming a NNE-SSW 250 km long ridge which comprises several major volcanoes such as Gago Coutinho, Ashton, Josephine and Jo Sister Seamounts (Fig. 5). To the south, the Gago Coutinho valley (GCV, Fig. 5) links to the main branch of the AGFZ and to an elevated area on which the Josephine submarine volcano formed.

4.2.1. Gago Coutinho volcano

The Gago Coutinho volcanic ridge consists of three submarine seamounts aligned along a N80°E direction that connects the AGFZ to the TAP (Fig. 5). Gago Coutinho (GC1), the largest and westernmost edifice is a complex E-W elliptical, steep sided volcanic edifice characterised by a flat summit narrowing from 9 km wide to the east to 3 km wide to the western end (Fig. 6a,b, Fig. 8b,c). The flanks of Gago-Coutinho have a distinct step-bench lava terrace morphology with an overall average slope of 40°, being steeper on the upper part of the flanks, decreasing to 15–20° near the base of the volcano (Fig. 6b, Fig. 8b,c). The northern flank displays several embayments at the summit with oversteepened scarps, convex shaped slopes, wide gullies and ridges and a wide bulge at the bottom front suggesting significant slope failure processes (Fig. 6b; Fig. 8c). To the east, U-shaped slope channels present two preferential E-W and NE-SW direction.

53 eruptive vents were identified mostly on the summit of the Gago-Coutinho edifice aligned along a NE-SW direction, oblique to the slopes (Fig. 6a, Fig. 11b). No vents were mapped on the southern steep flank.

4.2.2. Asthon submarine volcano

The Asthon submarine volcano (Fig. 7) displays a composite morphology including a large, 2300 m high, semi-circular and flat-topped volcanic cone, symmetrical with respect to a NE-SW axis, structurally linked to a NE-SW oriented topographic ridge (i.e. Asthon Ridge) to its SW. This ridge connects the main edifice to the nearby Gago Coutinho volcano via a saddle located at around 4500 m depth (Fig. 5, Fig. 8c).

Flanks of the main edifice display relatively moderate to steep slopes with average values exceeding 40° on the upper part of the flanks and 15–20° at the base of the edifice (Fig. 7b). The major slope break is located at ~1800 m similar to Gago-Coutinho. The general drainage pattern of the SE and NW flank of the Asthon main edifice is radial with alternating ridges and gullies extending from the summit to the seafloor (Fig. 7a). Sharp embayments are present at the summit suggesting significant slope failure processes.

One of the most prominent features in the NE flank of the volcano is the Asthon canyon, a flat-bottomed, N80°E oriented erosional feature extending from the top to the bottom of the volcano (Fig. 7a, Fig. 8a). It is about 10 km long, 2 km wide and bounded by steep (> 50°) and straight scarps. A series of broad longitudinal N80°E depression and ridges are observed near the base of the canyon. These volcanic ridges are also observed to the north in the same direction (Fig. 7a).

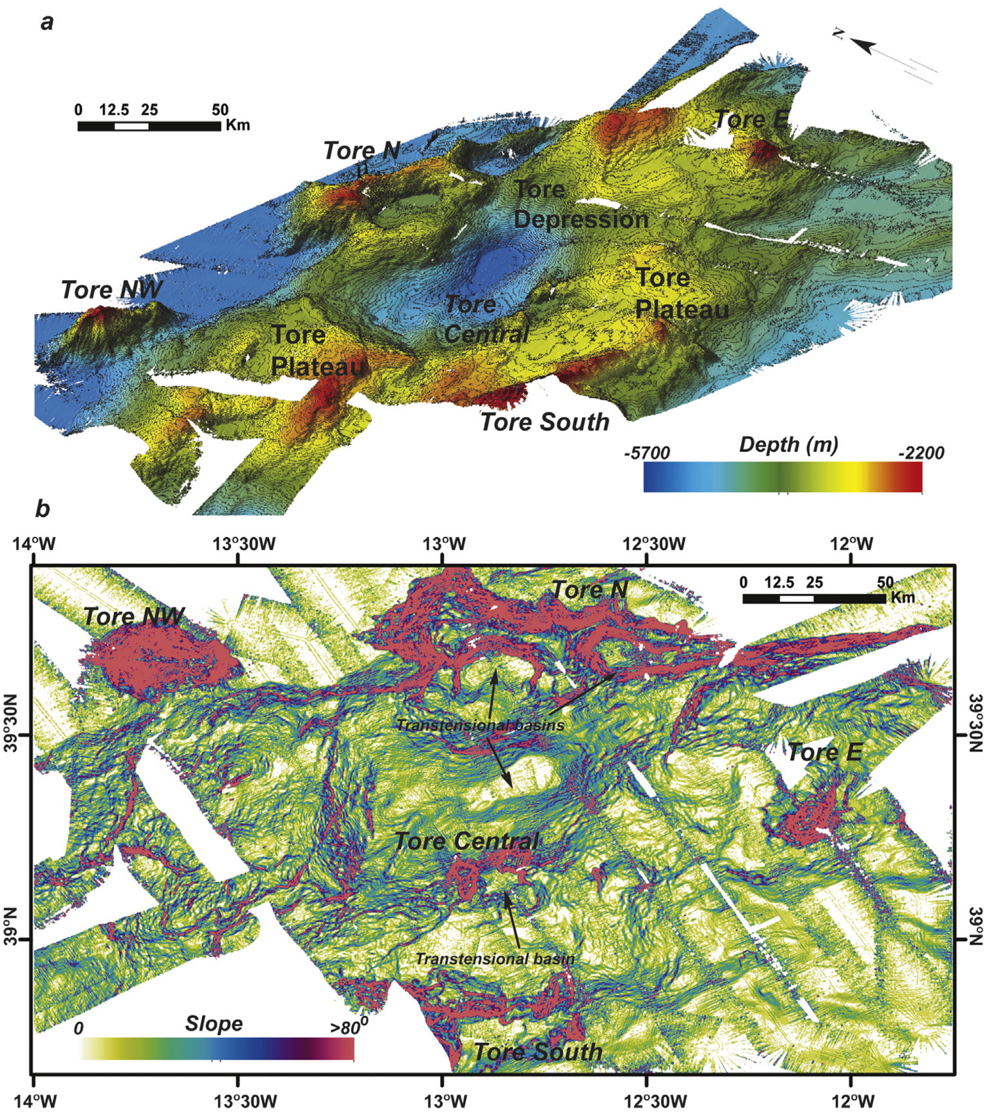

Fig. 3. a. 3D oblique view of the HR swath bathymetry of the Tore Volcanic Group localised to the north of Tore-Madeira Rise (Fig. 2) showing the main morphological and volcanic features. Bathymetric contours: 100 m and 20 m. Vertical exaggeration is x1.5. b. Slope distribution map of the Tore Volcanic Group.

The ~50 km long Asthon Ridge extending off the south-west side of the main edifice presents an en-echelon morphology with two preferential N*E*-SW and ENE-WSW orientations that connect to form one single ridge projecting to the main edifice (Fig. 7). The ridge displays a step-bench morphology related to repeated lava terraces emplacement.

Across the Ashton volcanic edifice, 30 eruptive vents were identified on the summit plateau and along the ridge (Fig. 7a, Fig. 11b) with a main alignment along a N45°E direction, defining a linear volcanic ridge zone. In addition, 12 vents aligned along a N20°E to N50°E direction were identified at the base of the southern flank, parallel to the Volcanic Rift (Fig. 7a, Fig. 11b). This may be related to fissure flank eruption. In the south-western part of the main edifice along the ridge, the eruptive fissures are oriented along two main directions N50–60°E and N0°E (Fig. 11b). To the south-western part of the ridge, elongated topographic feature on the seafloor can be observed along a N*E*-SW direction in the prolongation of the Ashton ridge and seem to connect with Gago Coutinho (Fig. 5, Fig. 8c).

4.2.3. Josephine and Jo Sister seamounts

Josephine and Jo Sister Seamounts are located to the south-west of the AGFZ and are part of large plateau with an average elevation of 2500 m above the seafloor (Fig. 2; Fig. 5). Only part of the edifices was imaged and most of the interpretation rely on the EMODnet DEM. The Josephine seamount is a 40 km long, flat topped summit, elliptic volcanic edifice with a NNW-SSE elongated axis, structurally linked to the AGFZ toward the north (Fig. 5). The southern flank is well imaged and displays two distinct ridges, one along a NNW-SSE axis direction with a length of 14 km and the other one with a WNW-ESE orientation with a length of 17 km separated by a large embayment (Fig. 5). 27 eruptive vents were mostly observed on the southern flank, with the exception of few vents mapped on the flat summit in the northern part of the edifice. To note, some of the eruptive vents may be undetectable due to the low resolution of the EMODnet bathymetric map or strong erosion imprint.

Two NNW-SSE elongated conical edifices can be observed to the northeast of Josephine along the AGFZ (VE1; VE2; Fig. 5). 13 eruptive vents are visible along the flank and the summit of the two volcanic edifices adjacent to the Josephine volcano (Fig. 5). Four eruptive fissures were identified with a WNW-ESE and NW-SE orientation similar to the cliffs localised to the NW (Fig. 11b).

Jo Sister seamount is located to the southeast of the Josephine plateau, south of AGFZ (Fig. 5). The edifice displays a square-like shape with three main peaks rising above a broad terrace at 1400 m depth surrounded by moderately steep flanks. The terrace may have once been the summit plateau similar to the other submarine flat-topped

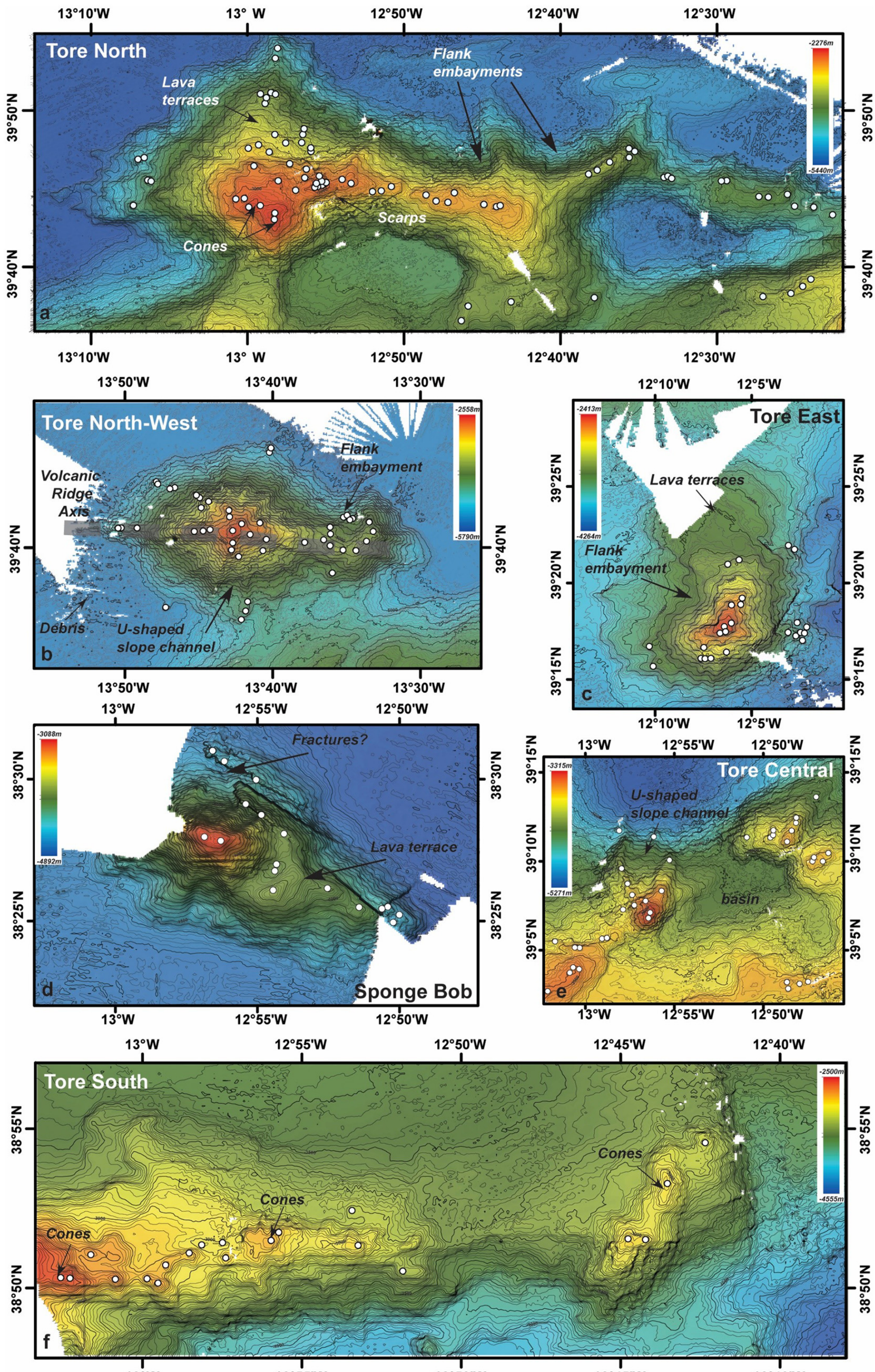

Fig. 4. High swath bathymetric map showing the morphology of the main volcanic edifices belonging to the Tore Volcanic Group as well as the isolated Sponge Bob volcano. White circle represents interpreted vents using the HR TOREMADERE bathymetry. Bathymetric contours: 100 m and 20 m.

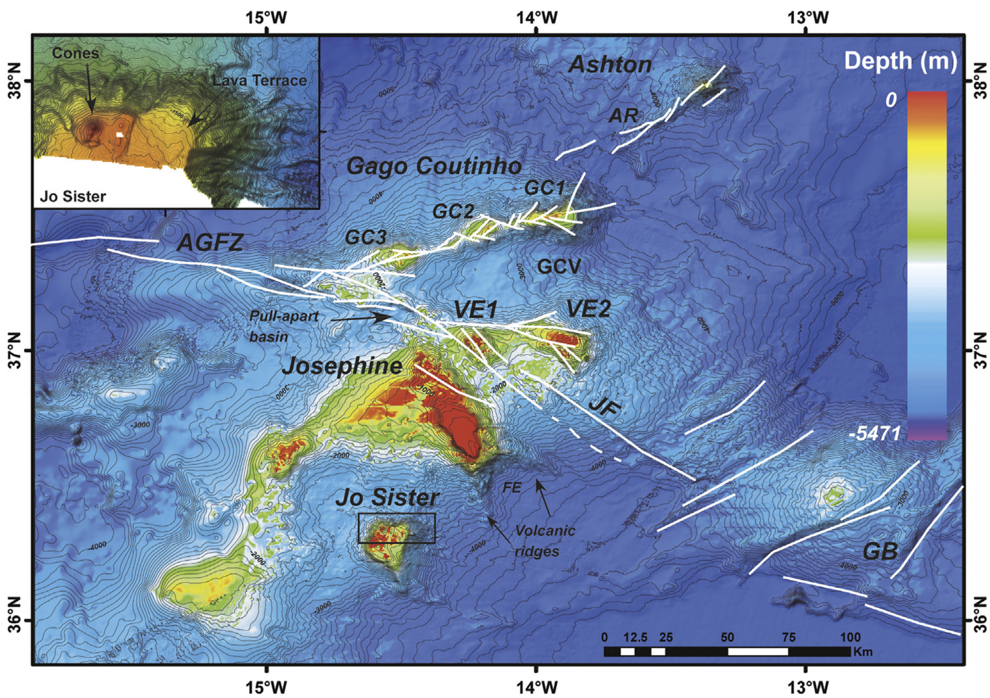

Fig. 5. Bathymetric map of the Central Volcanic Group localised along the eastern branch of the Azores-Gibraltar Fracture Zone (AGFZ). The main seamounts are Gago Coutinho, Ashton, Josephine and Jo sister. There are also, the Ashton Ridge (AR), three volcanic edifices of Gago Coutinho group (GC1, GC2, GC3), and other volcanic edifices (VE1, VE2). The Gago Coutinho Valley (GCV) is located between the Gago Coutinho group oriented ENE-WSW and the Josephine, VE1 and VE2 edifices. The Josephine Fault (JF) represents the south-eastern continuation of the AGFZ that links with faults along the Gorringe Bank (GB). Multi-beam TOREMADERE HR bathymetric data do not cover the entire area and edifices. Only 20% of Josephine (southern flank) and 40% of Jo Sister (the northern flank) seamounts were fully imaged. With respect to the large holes, the EMODnet regional bathymetric grid was used for regional interpretation. Bathymetric contours 100 m.

volcanoes, but small cones erupted aligned along a NN*E*-SSW direction on the northern and southern side. The base of the edifice lies on the seafloor at 2500 m depth in the north and 4000 m to the south in the abyssal plain.

4.3. Southern TMR Volcanic Group

The Southern TMR Volcanic Group is located to the south of the AGFZ (Fig. 2). The western branch is formed by a plateau-like rise (2500 m elevation) oriented NNE-SSW and capped by a volcanic edifice that is the Dragon seamount while the central part and the eastern branch include the Lion, Isabelle and Unicorn seamounts (Fig. 9).

4.3.1. Isabelle, Lion, Unicorn seamounts

The Lion Seamount shows a nearly E-W to NNW-SSE orientation with a summit at 600 m depth below sea-level. Bathymetry map shows that the ridge displays a series of WNW-ESE trending lineaments giving the ridge an en-echelon like shape with average spacing of ~6 km. The southern flank is nearly vertical with an average slope value around 50°. The northern flank is smoother and wider with a 15 km wide platform formed at an average depth of 1000–1500 m. Few isolated volcanic cones have also been mapped on both flanks of the ridge. The platform to the north gives away to two ridges oriented NNW-SSE and NNE-SSW. In the Lion seamount, 20 eruptive vents aligned along a WNW-ESE swarm of eruptive fissures similar to the bounded scarps can be identified at the summit.

The Isabelle Seamount is located to the east of the Lion Seamount. Its elliptical morphology is characterised by steep flanks and a flat summit (Fig. 9). Its elongation is oriented along a NNW-SSE turning to an E-W axis toward the NW near the Lion Seamount. The eastern flank of the volcanic edifice displays a well-defined large scarp facing toward the east.

Unicorn represents a N-S to NW-SE elongated volcanic edifice with a summit plateau located 800 m below sea level, south of the Isabelle and Lion volcanoes (Figs. 9, 10a). Its flanks are highly irregular resulting from the presence of numerous lava flows and possibly eccentric cones. Slopes range between 10° and 25° (Fig. 10b). The summit plateau is capped by several volcanic cones and surrounded by steep sided slopes that reach a terrace on its western flank at 1600 m depth (Fig. 10a). Distinct volcanic cones are preserved on the terrace. Although it was not fully imaged during the TOREMADERE marine survey, an additional volcano separated from the main edifice by a saddle is identified to the south-west of Unicorn (Fig. 10a). Massive lava flows are present along its southern flanks, reaching the abyssal plain at 4300 m depth.

108 eruptive vents were identified along the Unicorn edifice, mostly on the platform to the south and west of the summit (Fig. 9; Fig. 10a). These vents define a clear NNW-SSE oriented fissure parallel to the main elongation of the volcano, connecting to the Isabelle edifice to the north along which 10 eruptive vents aligned along a NW-SE direction were identified on the summit (Fig. 11c).

4.3.2. Dragon volcano

Dragon is located at the southwest end of the Southern Volcanic Group. It represents a N-S elongated volcanic edifice that up-domed the seafloor with a maximum height of 1500 m (Fig. 10c). It comprises two main well-defined N-S oriented ridge of 5 km wide separated by a bathymetric low saddle.

Dragon shows a rugged and uneven morphology with local irregular slopes ranging between 0° and 30° (Fig. 10d). Step-bench morphology with circular peaks located on the north-east and south-east flanks of the ridge at around 1800–1900 m above sea-bottom likely indicate the presence of flat-topped lavas terraces construction and development of small eruptive vents and volcanic cones. Large landslides are present in the central and north-western part of the ridge.

89 vents were recognisable along the Dragon volcanic edifice (Fig. 10c). The majority of the vents are aligned along N-S oriented eruptive fissures (Fig. 11c). To the north-east and south-east, eruptive fissures have a similar N-S trend but are shorter and separated by a large landslide suggesting that they might form part of the same eruptive fissure.

5. Faults identification

Criteria to define lineaments from bathymetry are mainly variations of the strike and offset of morphologically distinct linear features such as ridges, scarps, cliffs. The lineament drawn by following the bottom of the scarps were mapped and interpreted as related to faults.

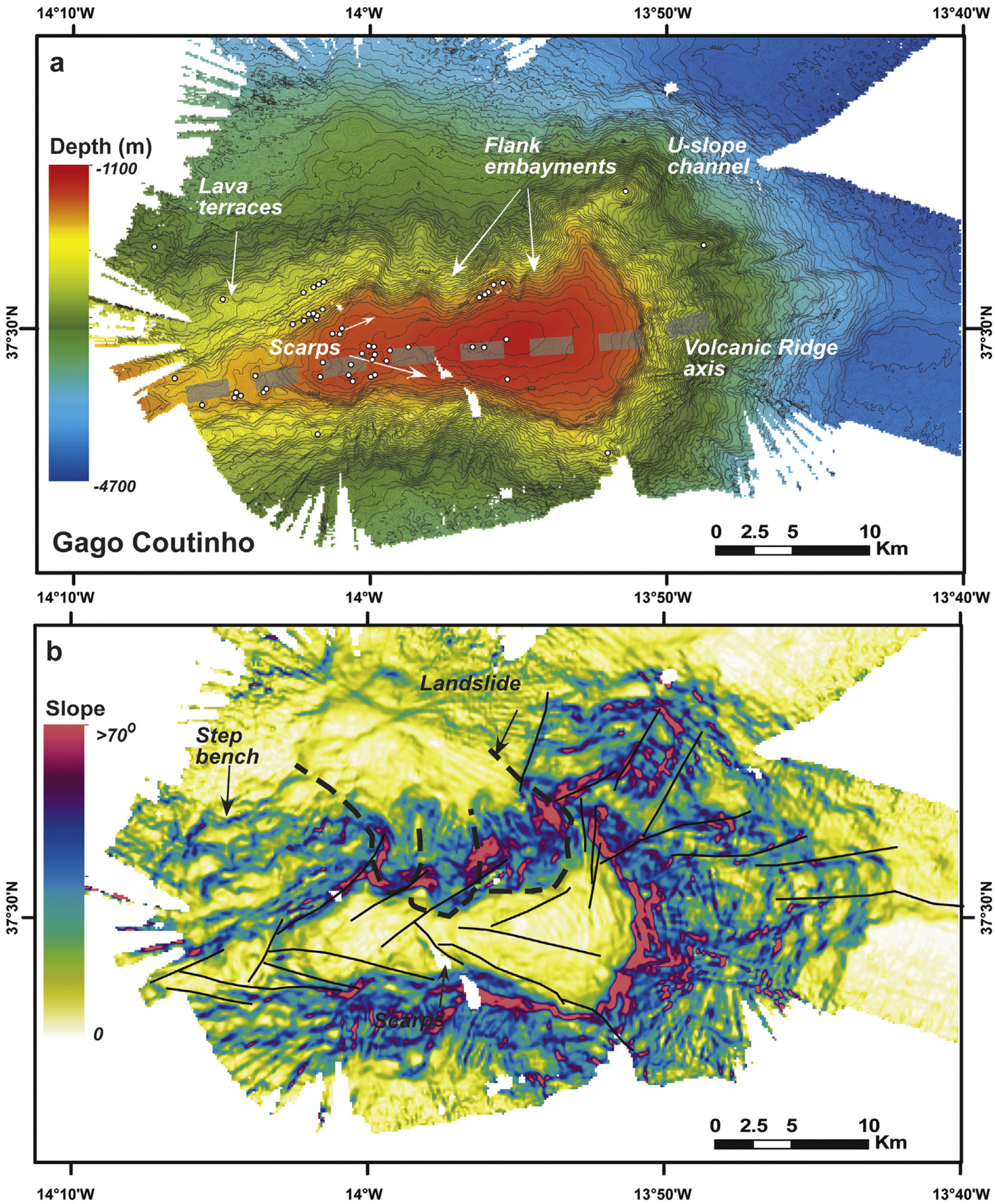

Fig. 6. (a) HR bathymetric and **(b)** slope distribution map of the Gago-Coutinho volcano (Central volcanic Group, location see Figs. 2 and 5). White circle represents interpreted vents. Bathymetric contours: 100 m and 20 m.

5.1. The Estremadura Fault System - the Tore Volcanic Group

The *E*-W faults of the EFS vanishes to the west into several en-echelon lineaments segments with a main N70°E and N50°E direction interrupted by N10°E striking lineaments (Fig. 3b; Fig. 11d). The westernmost part of the EFS and its splay faults have a clear bathymetric expression on the seafloor with a well-developed rhomb-shaped basin in the centre (i.e. Tore Depression) along releasing step-overs suggesting a left-lateral strike-slip component of the EFS (Fig. 3b; Fig. 11d). The two major splay segments surrounding the Tore Depression and where the Tore N and Tore Central lie also show small NE-SW oriented transtensional basins surrounded by ENE-WSW to NE-SW strike-slip faults that step across along NNW-SSE faults (Fig. 3; Fig. 11d).

5.2. The Azores-Gilbratar Fracture Zone – Josephine Volcanic Group

HR bathymetric data and EMODnet DEM were used to map the main lineaments along the AGFZ. The eastern part of the AGFZ, along which the Josephine Seamount Group lies, is composed of several fault segments mostly striking N80–120°E and splays off eastward into two main fault sets forming a horsetail geometry (Fig. 5).

The main sub-vertical fault oriented N110–120°E has a length of 50 km splitting into four smaller steep secondary faults, 40 km–60 km long with an orientation ranging between N120°E to N150°E. A zone of transtension developed along this main segment as expressed by the presence of small pull-apart basins as well as the localisation of the Josephine Volcanic Group. Typically, the different volcanic edifices of the Josephine Volcanic Group are located either at the tip of the main fault or along the several splays of oblique faults (Fig. 5; Fig. 11e). Beyond the south-eastern end of the AGFZ splay faults, the seafloor

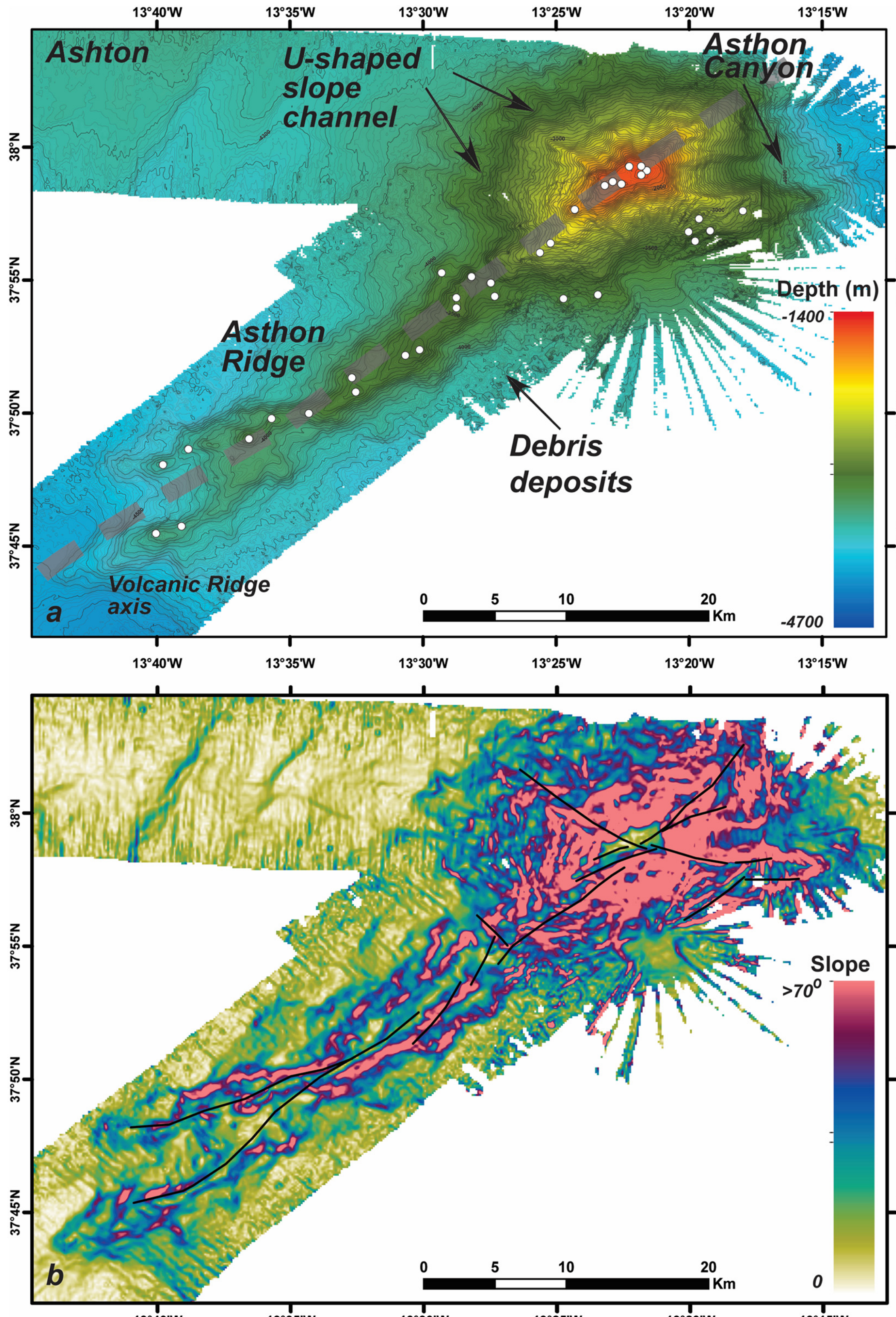

Fig. 7. **(a)** HR bathymetric and **(b)** slope distribution map of Ashton volcano (Central volcanic Group, location see Figs. 2 and 5). White circle represents interpreted vents. Bathymetric contours: 100 m and 20 m.

fabric related lineaments strike N50°E (Fig. 5; Fig. 11e). At the junction with the N130°E AGFZ system, these individual N50°E lineaments change their geometry along a strip-oriented NW-SE (the Josephine Fault; Fig. 5; Fig. 11e) that is in the south-eastward continuation of the AGFZ splay faults. These NW-SE lineaments that have a different direction define two linear corridors in the bathymetry where each individual segment displays a left-lateral stepping geometry (Fig. 11e). These corridors are sub-parallel converging to a small edifice of the Josephine Volcanic Group located at the tip of one of the AGFZ splay fault. (VE1 in Fig. 5; Fig. 11e).

The northern segment of the AGFZ splay faults consists of several small, 20 km long, NE-striking, right lateral stepping cracks linked by a

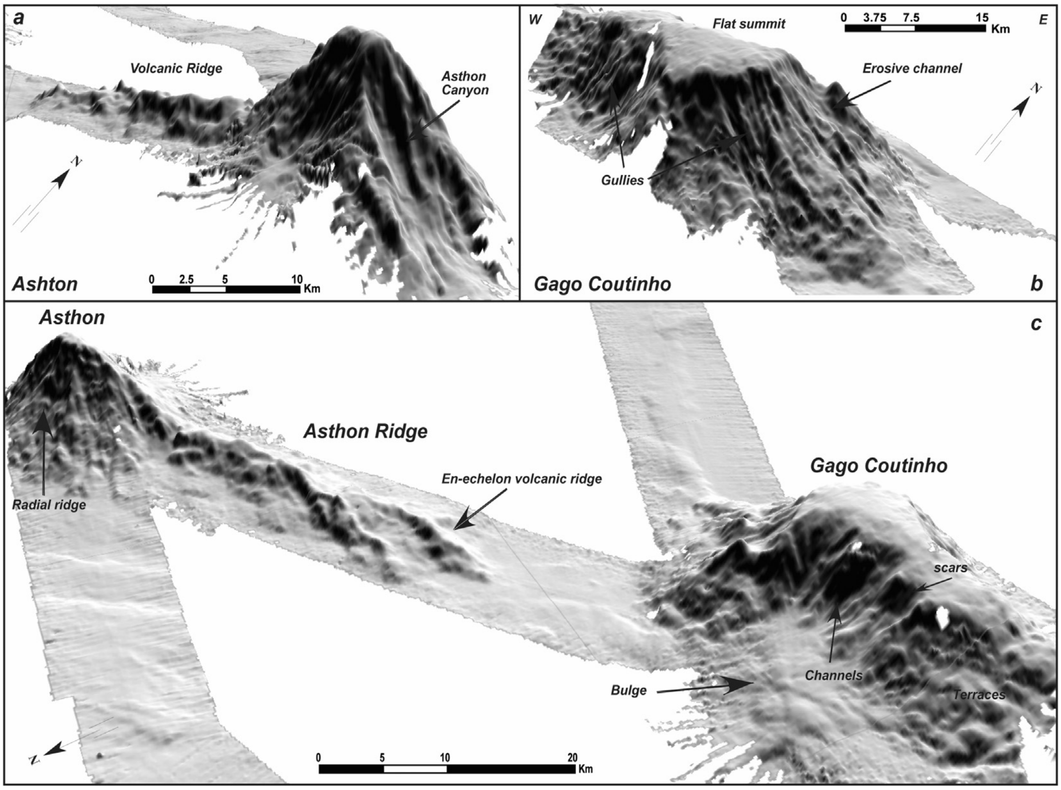

Fig. 8. 3D images of **(a)** the Asthon volcanic edifice (view to the NW), **(b)** the Gago Coutinho volcano (view to the NW) and **(c)** the Asthon Ridge that connects the two main edifices (view to the SE). Vertical exaggeration is x1.5.

set of overstepping N100–105°E oriented fault segments (Fig. 5; Fig. 11e). However, their trend is not parallel to the predicted orientation for antithetic faults. Instead, these faults strike parallel to extension fracture. These set of faults is well expressed in the morphology of Gago-Coutinho in the form of WNW-ESE trending, and NE-SW-trending, vertical en-echelon fault related lineaments that localised slope deformation on its flanks and summit (Fig. 6). The left-lateral fault segments linked through extensional overstep defining a staircase-shaped fault zone with extension fractures, pull-aparts striking N40–50°E along which the Gago-Coutinho Volcanic Ridge developed. The NE-SW fractures of the Gago Coutinho volcanic edifice likely branches to the NE-oriented fault well expressed in the bathymetry by the strike of the Ashton Ridge.

5.3. Southern TMR

The Southern TMR lineaments have a length of 20-40 km and cover an area of 40 km wide (Fig. 11f). The fault system in the vicinity of the Dragon seamount is formed by two parallel N-S faults branching to the north and south to roughly *E*-W transform faults. The strike of the rift valley related normal fault are also N-S suggesting that the fractures observed on bathymetry and along which the Dragon lavas formed are

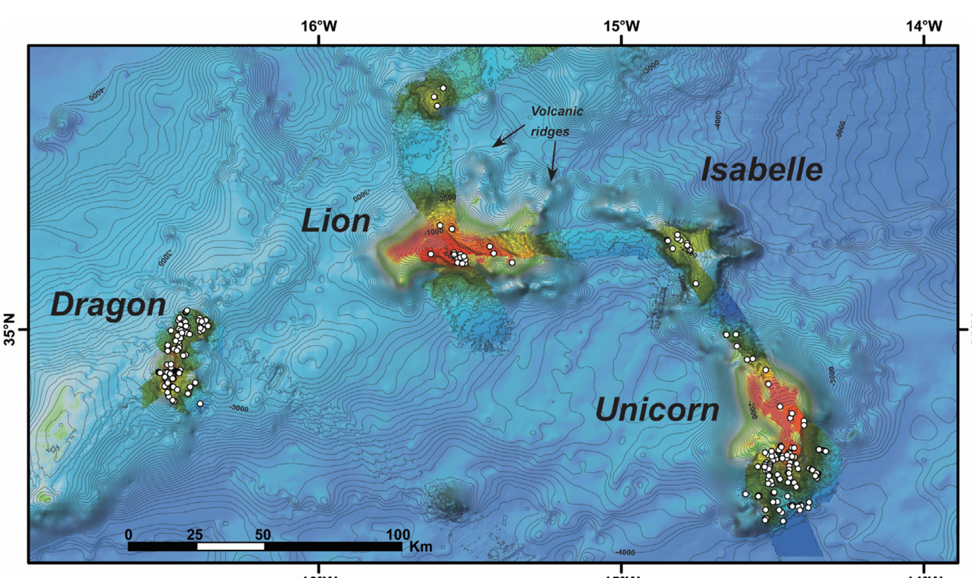

Fig. 9. Bathymetric map of the Southern Volcanic Group. The main seamounts are Lion, Isabelle, Unicorn and Dragon. White circle represents interpreted vents. The HR bathymetric data only covers 20% of the area along the main edifices. The EMODnet regional bathymetric grid shown in the background was used for regional interpretation.

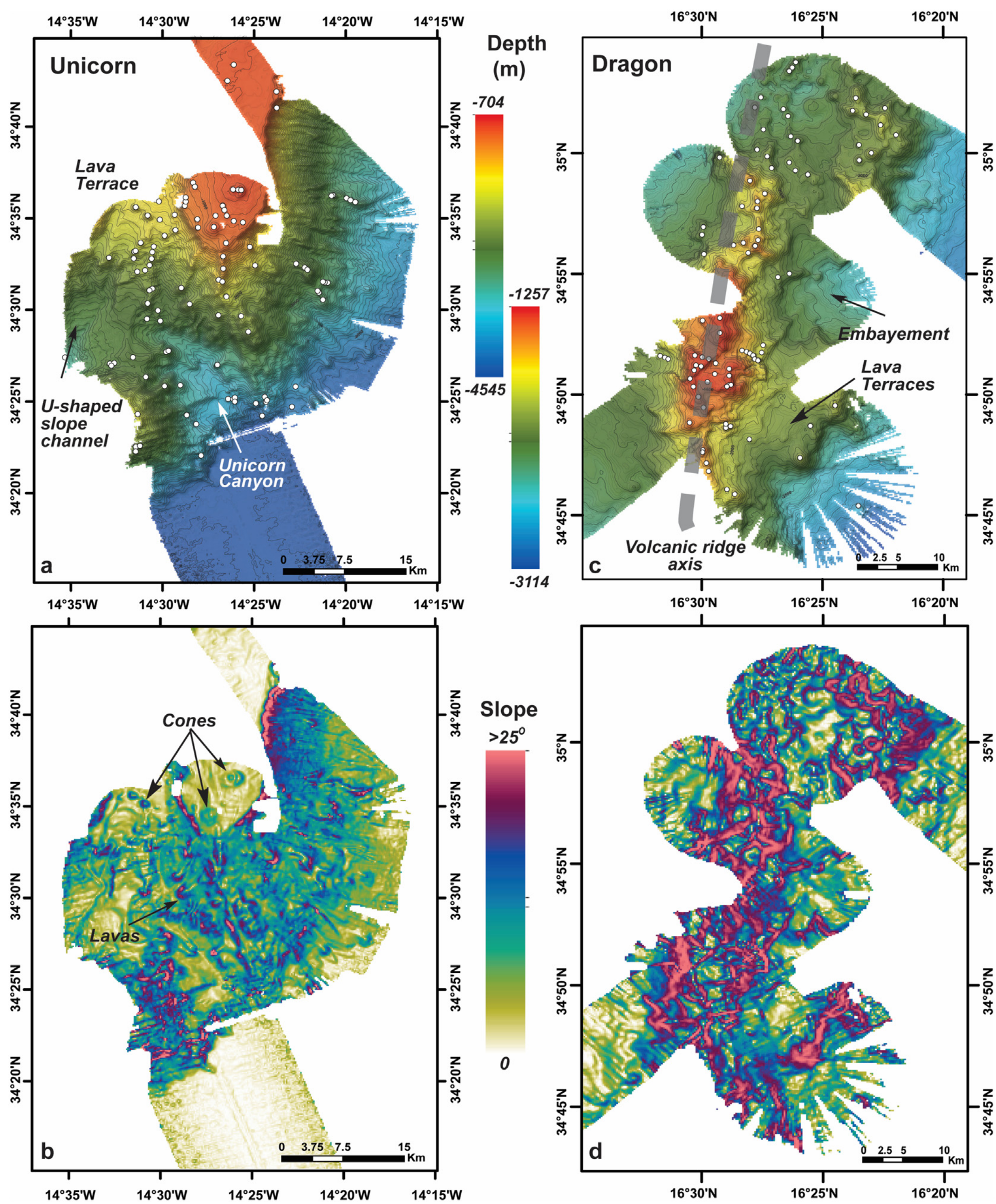

Fig. 10. HR bathymetric and **(b)** slope distribution map of the **(a)** Dragon and **(b)** Unicorn volcanic edifices (Southern Volcanic Group, location see Fig. 2, Fig. 9). White circle represents interpreted vents. Bathymetric contours: 100 m and 20 m.

reactivated normal faults formed during the oceanic spreading.

The Lion-Isabelle area consists of NW-SE right stepping en-echelon lineaments curving to the east in the Lion volcano and to the west in the Isabelle edifice and connecting to an E-W fault (Fig. 11f). This latter is well expressed in the bathymetry with a large vertical offset of the seafloor fabric as shown on the slope map (Fig. 11f). To the east, the transform fault is cross-cut by structures of Isabelle oriented NW-SE curving westward to the north and connecting to the NNW-SSE structures of Unicorn.

6. Discussion

6.1. Morphostructures and spatial distribution of volcanic edifices along the TMR

The difference in the overall morphology of the submarine volcanoes along the TMR is likely related to magma supply rate and chemical composition, structural inheritance of the lithosphere on which the volcanoes are lying, submarine or subaerial conditions for volcanic emplacement, gravitational flank instabilities and erosion processes (e.g. Ramalho et al., 2013). Our new bathymetry data provide new insights to identify these processes and assess how they contributed to the morphology of the volcanoes as observed nowadays.

The most striking morphological feature of the TMR seamounts is that steep-sided, flat topped summit and lava terraces can be observed on almost all the volcanic edifices whatsoever their size. The presence of flat topped cones with lava terraces from the base to the top of the edifice may be explained primarily by submarine volcanic construction processes. Long-lived eruption of low- to moderate viscosity lavas (i.e. OIB-like alkaline basalt and trachybasalt, Merle et al., 2009) in a deep-water environment may favour the development of flat summit and terraces as suggested for some oceanic seamounts in the Pacific (Clague

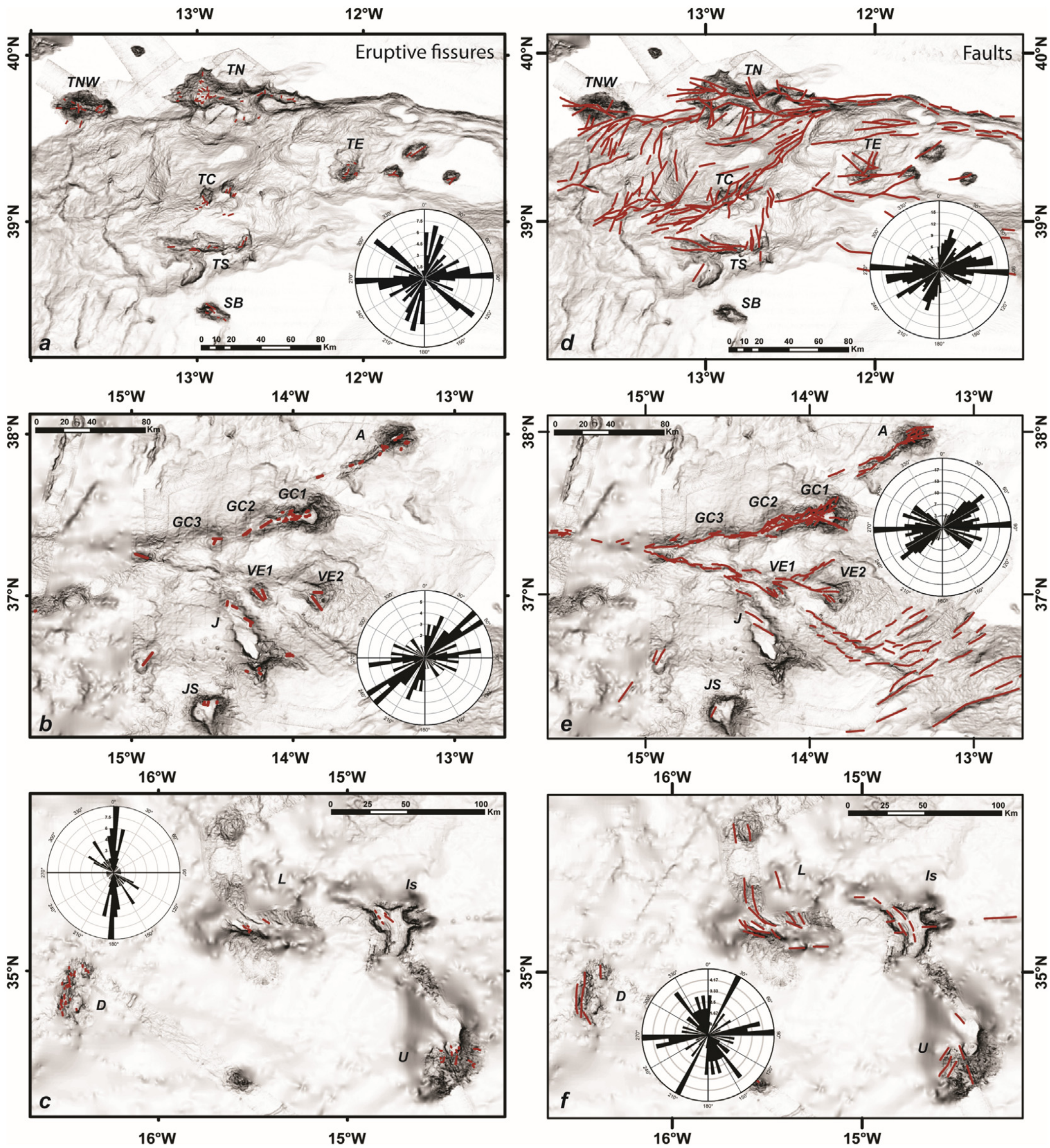

Fig. 11. Distributions of the main bathymetric features including interpreted volcanic eruptive fissures as well as fault related lineaments of the (a, d) northern, (b, d) central and (c, e) southern volcanic groups: Rose diagram showing the azimuth frequency of interpreted volcanic eruptive fissures and fault related lineaments. A: Asthon, D: Dragon, GC1, GC2, GC3: Gago Coutinho, Is: Isabelle, J: Josephine, JS: Jo Sister, L: Lion, SB: Sponge Bob, TC: Tore Central, TE: Tore East, TN: Tore North, TNW: Tore North-West, TS: Tore South, U: Unicorn; VE1, VE2: volcanic edifices.

et al., 2000). In such case, the small volcanic cones observed on summit or flank plateaus (i.e. Unicorn and Jo Sister) likely represent late- or rejuvenated stage volcanism. Flat-topped volcanoes may also result from subaerial erosion processes such as waves action upon the edifices (Paduan et al., 2009). Although some volcanoes may have reached the surface or the summit were near sea-level fluctuations (i.e. Josephine, Unicorn), no clear evidence of past subaerial conditions such as beach deposits or guyot morphology can be observed based on the HR bathymetric data.

The overall shape of these volcanic edifices is variable across the TMR with ellipticity values ranging between ~0.26 and ~0.86 with > 70% of the values higher than 0.5 (Table 1). Although post-emplacement erosional processes such as slope failure or canyon incision (Mitchell et al., 2002) may have affected the ellipticity to some extent (i.e. northern flank of Gago Coutinho volcano), destruction processes may not affect the entire edifice and the ellipticity should reflect the primitive shape of the volcanic edifices. This large variation of ellipticity suggests different types of volcanic constructions (Fig. 12). Small ellipticity are likely related to fissure eruptions along pre-existing structures (i.e. Tore Central, Dragon) while medium to high ellipticity are consistent with sub-circular seamounts reflecting locally focussed volcanism during long-lived eruptions (i.e. Gago Coutinho, Tore N). Both morphologies may represent the evolution in eruption style through time from early eruptions along pre-existing faults to more point focussed eruptions on a mature edifice. Variable local stress along the fault system may also result in different morphologies. Examples of the co-existence of both morphologies can be observed on the Asthon volcano which is composed of a main NE-elongated, semi-circular, flat-topped and terraced edifice with a SW-trending sharp linear en-echelon ridge on its south-eastern slope (Figs. 7 and 8).

The detailed mapping of volcanic occurrences distribution together with structural analysis of the bathymetry at regional-scale show that most of the volcanic fields are located within different crustal domains (oceanic or exhumed mantle) in the vicinity of major sub-vertical lithospheric structures such as transfer faults of the margin, oceanic transform faults or former mid-oceanic spreading ridge (i.e. AGFZ, EFS; Fig. 2). For instance, the Tore and the Central Volcanic Groups display NE-SW to E-W trending elongated volcanoes as illustrated by the main

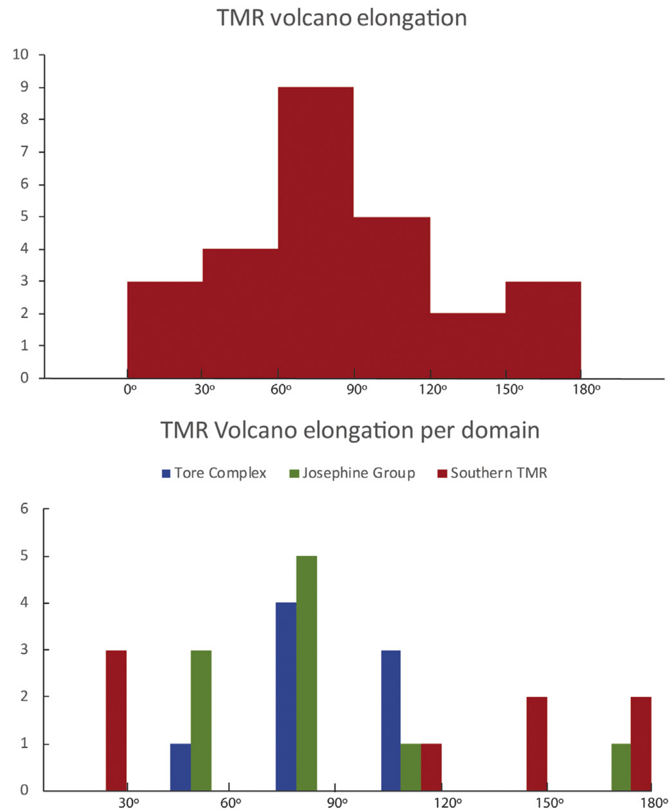

Fig. 12. Orientation of the elongation of the volcanoes (a) along the Tore-Madeira Rise and (b) per volcanic groups.

axis of the volcano ellipticity. This overall trend is parallel to the main direction of the rift-related normal faults and transfer zones along the Iberia margin (Fig. 2; Fig. 12; Tucholke et al., 2007). Intrusives and volcanoes of similar age and composition as the Tore Volcanic Group and Josephine Volcanic Group are also present 300 km away from the TMR volcanoes in the Tagus Abyssal Plain and onshore Portugal (Miranda et al., 2009; Grange et al., 2010; Neres et al., 2014). These intrusives have also a preferred *E*-W to NE-SW orientation similar to the TMR edifices and were emplaced in the vicinity of main lithospheric faults (Messejana and Nazaré faults). Structural studies of the Iberia margin evidenced pre-existing *E*-W and NE-SW fault systems formed long before the beginning of the magmatic activity on the TMR during the Late Paleozoic Hercynian Orogeny and controlled margin segmentation during the Early Mesozoic rifting event (Fig. 1; Alves et al., 2009; Ballevre et al., 2014; Pereira et al., 2016). This clearly demonstrates the strong structural control on the location of Tore and Central Volcanic Group as pre-existing lithospheric structures influenced the main magmas ascent pathways. The absence of a major N-S oriented axis of the TMR volcanoes in the central and northern part of the seamount chain contrasts with the inferred N-S to NNE-SSW orientation of the overall TMR. We thus suggest that the spatial distribution of the TMR volcanoes reflects the channelling of magmas into sub-vertical lithospheric faults rather than a N-S to NNE-SSW plate motion over a hot-spot (e.g. D'Oriano et al., 2010). We also estimate that the limited structural connection along a N-S transect of the TMR volcanoes and the presence of three distinct volcanic fields (i.e. Tore Volcanic Group, Josephine Volcanic Group and Southern Volcanic Group) does not support the concept of an age decreasing hot-spot track and highlights the misleading of the term “Tore-Madeira Rise” in such complex poly-phased tectono-magmatic context.

6.2. Mechanism of magma channelling and ascent

Faults along which volcanoes formed consist of several kilometric-scale sub-vertical segments mainly oriented N0 and N90°E in the southern part of TMR, N90°E, N120°E and N40°E in the central part along the AGFZ and in the Tore Seamounts Group area (Fig. 12). Although some volcanoes might have been buried beneath a thick sediment package and a large volume of underplated magmatic bodies or sills are likely present beneath the distal part of the Iberia margin or intruded within the oceanic lithosphere beneath the southern part of TMR (Peirce and Barton, 1991; Pereira et al., 2016), the TMR volcanoes appear to be spatially clustered and located only on a small portion of the sub-vertical pre-existing fault system (Fig. 13). In addition, the majority of these volcanoes are located away from the major segments of these regional faults (i.e. shaded grey area; Fig. 13) suggesting that a structural control on volcanic emplacement is more complex than previously suspected (Geldmacher et al., 2006; Merle et al., 2006; Nirrengarten et al., 2017).

Transport of melt by fault zones greatly depends on fault-zone structure and permeability within the damage zone (e.g. Gudmundsson et al., 2010). Indeed, structural and rheological complexities of fault damage zones strongly perturb regional tectonic stresses along, across and around the damage zone which favour the development of sub-domains with different deformation pattern, fault geometries, kinematics and permeability as well as stress regime (Choi et al., 2016; Ishii, 2016; Peacock et al., 2017). The development of damage zone also results in strong rock anisotropy between the weaker and more permeable fault damage zone and the surrounding host rocks. This strength contrast results in pressure gradient between the fault zone and the host rock and may induce magma to ascent (Gudmundsson et al., 2014; Reynolds et al., 2018). Alternatively, magma-assisted processes enhancing fracturation is another process that may favour magma to flow (i.e. Hydrofracturation, Gudmundsson and Brenner, 2001). In such scenario, magma pressure is sufficiently high to inject dyke to the surface creating local extension in the shallow crust (Accola, 2014; Ruch et al., 2016).

Considering the localisation of large volcanic edifices within sub-vertical lithospheric faults without any evidence of morphological offset, (diking) fracturing controlled by the pre-existing fault zone is likely the mechanism that favoured pathways for magma to ascent. In such scenario, the steep dip of the fault gives to the sub-lithospheric melts a direct access to the surface. However, the majority of the volcanoes of the Tore and Josephine Volcanic Groups studied here, did not develop directly on the major regional fault but rather along sub-ordinate or splay faults suggesting a strong control of tectonic local stress in regard to fault geometry (Fig. 13). Moreover, although the average strike of eruptive fissures and faults are nearly concordant, the pattern of the eruptive fissure presents two or more preferential directions (Fig. 11). In fact, most of the volcanoes of the TMR formed on a lithosphere with a complex structural geometry including, releasing bend zones defining a transtensional domain (Tore Volcanic Group), at the interaction or tip damage zone of the splay faults (Josephine Volcanic Group, Gago Coutinho and Ashton Seamount), and failed proto-spreading ridge interacting with transform fault (Lion, Isabelle). Based on these observations, we suggest that local stress reorganisation exerted a primary control on magma ascent toward the surface and the site of emplacement of the TMR volcanoes. The complexity of the fault systems favoured the development of sub-domains between and at the tip of different fault segments that when optimally oriented to minimum horizontal stress would enhance magma ascent and allow eruption at the surface.

6.3. Control of the local stress field on TMR volcanism

The EFS splays off to the west in several segments-oriented N*E*-SW defining a horsetail-like system of sinistral faults along which the Tore

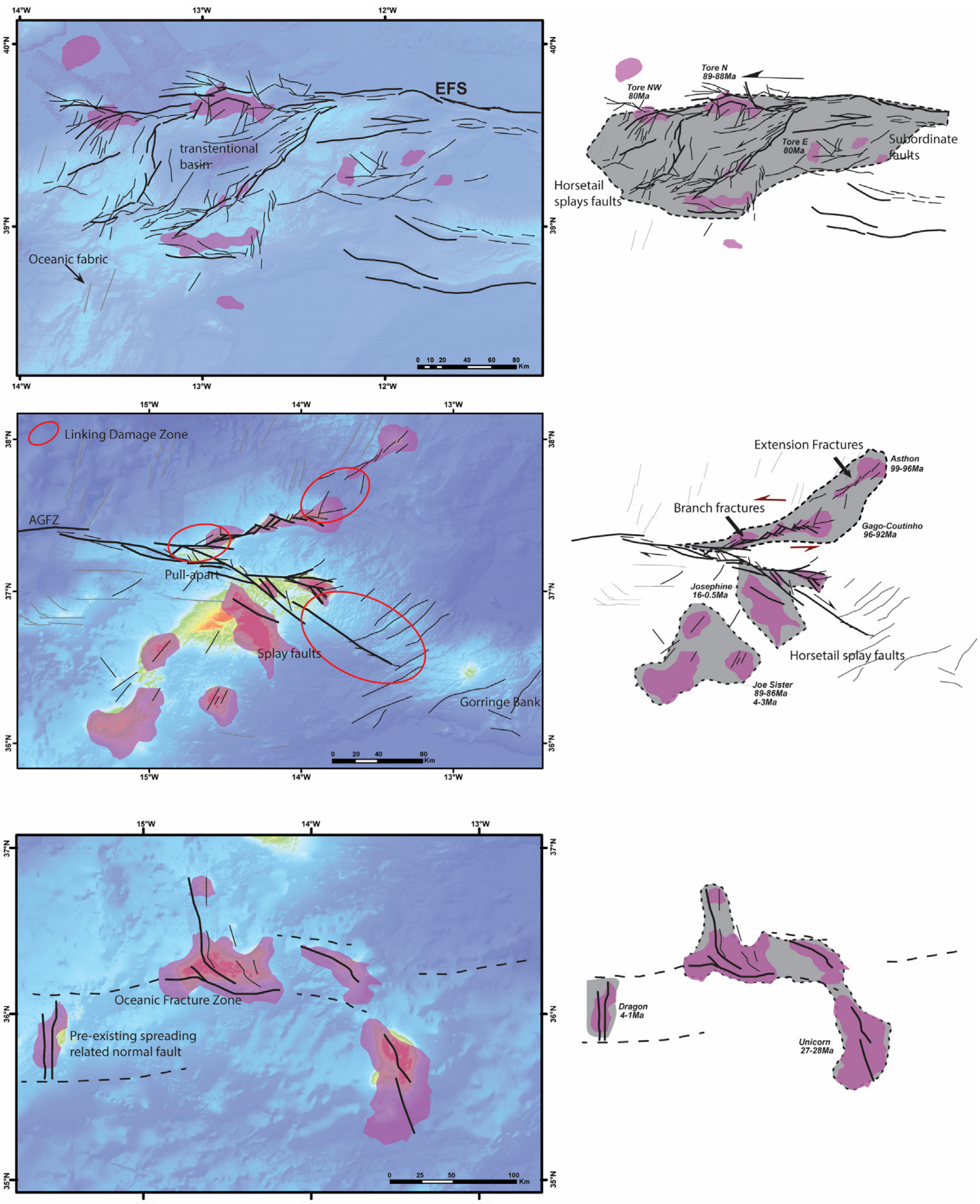

Fig. 13. Tectonic maps with distribution of volcanoes of the (a) Tore Volcanic Group, (b) Central and (c) Southern domains. Thick black line = major black faults, thin black line = minor faults. Light grey lines correspond to the main seafloor fabric. Light grey dotted shadings indicate tip or interaction damage zones along which the main volcanoes formed (purple polygons). (For interpretation of the references to colour in this figure legend, the reader is referred to the web version of this article.)

depression formed (Fig. 13). The western tip of the EFS where the Tore Volcanic group developed is interpreted as being structurally and kinematically linked to left lateral strike slip faults located in the distal and proximal domains. These latter acted as steep E-W transfer faults during continental rifting and were likely reactivated in a transtensional regime after rifting and spreading ceased (Pereira et al., 2016).

Most of the volcanoes of the Tore Volcanic Group developed within the transtensional domain of the EFS (shaded grey zone in Fig. 13). Eruptive fissures are either sub-parallel or oblique to the main ~E-W oriented segments and NE-SW splays of the EFS. Both trends are compatible with a sinistral transtensional regime. This structural configuration indicates that magma transport and eruption are driven by subordinate or horse-tail splay faults. The transcurrent deformation and potentially associated rotation of the stress field along the EFS would favour the opening of these faults and melt emplacement in localised area of transtension (Fig. 13). The complex pattern of eruptive fissures within the Tore N, Tore NW and Tore Central are prime examples of these processes. Cone elongation and associated eruptive fissures strike dominantly ENE, NNE and SE and are thus likely a mixture of shear and extensional fractures considering the sinistral strike-slip character of the main fault and its splays. The sub-vertical lithospheric EFS likely rooted to deep crustal level thus provided access to the main source of magma.

The Josephine Volcanic group is located at the vicinity or along the eastern part of AGFZ (Figs. 5, 13b). This latter represents a ~E-W transform plate boundary between the North and Central Atlantic

Oceanic plate changing to a more complex NW-SE and NE-SW oriented transform margin toward the east between the Iberian and African plates (e.g. Jiménez-Munt et al., 2001). The structural analysis along the N80°E segment of the AGFZ where the Gago Coutinho volcanic edifice emplaced shows that fault related lineaments are arranged in a NE-SW right-stepping en-echelon segments linked up by E-W to WNW-ESE faults that define a zigzagged trace. The NE-SW segments coincide with mapped eruptive fissures within the Gago-Coutinho edifice as well as match the spatial distribution of the three volcanic edifices that composed the Gago-Coutinho Ridge along this segment of the AGFZ (Figs. 11 and 13).

This geometry suggests that WNW-ESE oriented segments correspond to shear fractures that interacted, creating NE-SW extensional fractures along which magma erupted as suggested by the pattern of eruptive fissure (Fig. 13b). In that configuration, Gago Coutinho (Fig. 13b) is located at the tip damage zone of the AGFZ. The large volume of the volcanic ridge indicates that the fault was reactivated by repeated movement, creating a complex and high concentration of fractures enhancing melt extraction and triggering volcanic eruption.

The Ashton volcano developed along a NE direction and presents a ridge that potentially connects to Gago-Coutinho at depth although it is not clearly observed on the bathymetry (Fig. 5, Fig. 8c). However, the strike of the ridge is similar to the NE-oriented fractures and eruptive fissures of the Gago-Coutinho Ridge that are interpreted as being extensive fracture-related dykes. The Asthon volcano shows a dyke swarm tip-crack geometry as well as en-echelon spatial distribution of eruptive fissures compatible with a sinistral shear component during volcanic building. Thus, we propose that the Asthon volcano developed along extension fractures formed at the tip of the AGFZ–Gago Coutinho left-lateral shear fault segment. In such tectonic context, the contrasting morphology between the ridge and the main edifice may be explained by fissure eruption along a pre-existing fracture followed by long-lived eruption and edifice growth at the damage tip of the fracture.

Similarly, the eastern portion of the AGFZ hosts the Josephine Volcanic Group (Fig. 13b). Right-lateral shear along this portion of AGFZ is predominantly accommodated along NW-SE to WNW-ESE trending dextral horsetail splay faults. Most of the volcanic edifices localised at the fault tips or along en-echelon shears where the AGFZ changes direction and connects to the NE-SW trending lineaments of the Gorringe Bank (Fig. 13b). This new kinematic configuration thus reorganised the local stress along pre-existing segments of AGFZ and controlled the localisation of the Josephine Volcanoes.

6.4. Implications for the post-spreading deformation of the Iberian margin

The proposed model of the TMR volcanism questions the localisation of the segmented N-S to NNE-SSW oriented J-magnetic anomaly that is laterally offset by transform faults (Bronner et al., 2011). Indeed, the E-W structural trend of post-spreading volcanoes differs significantly from the inferred N-S trend of the J-anomaly (Fig. 2; Fig. 13). Recently, Nirrengarten et al. (2017) interpreted this anomaly as the result of polyphased *syn*- to post spreading magmatic events emplaced in both the oceanic and exhumed mantle domains. We thus speculate that this configuration may be related to relicts of underplated magma emplaced along detachment faults and channelizing toward the major sub-vertical lithospheric faults (Sauter et al., 2018). This also may suggest that migration and extraction of melt to the surface is more efficient where steep lithospheric shear zones such as transfer or oceanic fracture zones associated with local stress variations are present.

Post-spreading deformation occurred along two major fault zones (i) the ~E-W to ENE-WSW oriented EFS to the north that splays off southwestward to connect to (ii) the E-W to NW-SE AGFZ in the southern part of the Iberia margin (Fig. 2). These structures formed obliquely to the main NNE-SSW oriented seafloor oceanic fabric and shows mainly left -lateral displacement evidenced by the development of transtensional and pull-apart basins (Fig. 13). Deformation likely began at least in the late Early Cretaceous based on the age of the earliest stage of post-spreading volcanism that emplaced along these faults (i.e. 103–96 Ma, Merle et al., 2006). The direction of main stress at that period changed from NE-SW to ~E-W according to direction of the flow lines obtained by reconstruction of the Iberia-Newfoundland margin (Nirrengarten et al., 2018). During this period, a triple junction between the Bay of Biscay, Ireland and Newfoundland initiated to the north (Nirrengarten et al., 2018), turning the early margin related transfer faults into transtensional to extensional faults. In such configuration, we propose that rotation related extension (transtension) along the SW Iberia margin would have caused the magmas to be drained along major pre-existing oceanic fractures and transfer faults of the Iberia margin and triggered eruption of submarine TMR volcanoes during the Late Cretaceous. Furthermore, deformation localised along these major lithospheric fault zones show large crustal thickness and thermal variations inherited from the Late Variscan Orogeny and Mesozoic rifting (Tesauro et al., 2009; Veludo et al., 2017). Thus, these structures represent major crustal boundaries that mostly reactivated inherited Late-Variscan basement boundaries and lithospheric shear zones. These fault zones acted as boundaries accommodating the differential plate motion between the fragmented Iberian and African plates, enhancing post-spreading deformation and volcanism across them at times of plate reorganisation.

7. Conclusions

The analysis of the new HR bathymetric data combined with regional DEM of the TMR reveal post-spreading deformation processes associated with magmatic emplacement along the Iberia-Morocco margin. The main conclusions are as follows:

1. The TMR consists of three distinct major volcanic massifs, the Tore Volcanic Group, the Josephine Volcanic Group and the Southern group complex that are spatially connected to respectively, major regional faults such as EFS and AGFZ along the SW Iberia margin and a former ridge-transform system, offshore Morocco. These large pre-existing lithospheric-scale shear zones likely acted as preferential pathways for the ascending magmas.
2. Magma transport and eruption are overall controlled by the local state of stress along pre-existing faults. Only specific portion of the faults including splay fault releasing bend, fault tips and interaction zones between two segments are coated by large volcanoes. Volcanic emplacement varies through time depending on the change in plate kinematic. This suggests that magma migration requires local stress reorganisation induced by complex fault geometry and fault segment interaction to erupt. Other control parameters include (i) the steep dip of the faults that directly tap into the molten source and, (ii) the rheological weakness of the shear zones;
3. Development of a transtensional plate boundary during the Late Cretaceous likely resulted in post-spreading magma emplacement in the southern part of the Iberia margin. Plate reorganisation resulted in the transition to intense right-lateral shearing along the AGFZ is well expressed by the distribution of TMR volcanoes.

Acknowledgements

This work is based on the data collected during the TOREMADERE cruise (https://doi.org/10.17600/1010110) in 2001. We thank the captain and the crew of the R/V *Atalante* for their professionalism during the cruise. We also acknowledge the early work of Jacques Malod, Luis Matias and Luis Pinheiro for data acquisition and processing onboard and early interpretative discussions. For technical assistance we thank E. Boeuf, B. De Quillac and H. Loyen. We are grateful to two anonymous referee and Michele Rebesco for their constructive remarks and editorial work.

References

Accola, V., 2014. Structural control on magmatism along divergent and convergent plate boundaries: Overview, model, problems. Earth Sci. Rev. 136, 226–288.

Afilhado, A., Matias, L., Shiobara, H., Hirn, A., Mendes-Victor, L., Shimamura, H., 2008. From unthinned continent to ocean: the deep structure of the West Iberia passive continental margin at 38°N. Tectonophysics 458, 9–50.

Alves, T.M., Abreu Cunha, T., 2018. A phase of transient subsidence, sediment bypass and deposition of regressive-transgressive cycles during the breakup of Iberia and Newfoundland. Earth Planet. Sci. Lett. 484, 168–183.

Alves, T.M., Moita, C., Cunha, T., Ullnaess, M., Myklebust, R., Monteiro, J.H., Manuppella, G., 2009. Diachronous evolution of Late Jurassic–Cretaceous continental rifting in the Northeast Atlantic (west Iberian margin). Tectonics 28, TC4003. https://doi.org/10.1029/2008TC002337.

Applegate, P., 2003. Detection of sinkholes developed on shaly Ordovician limestones, Hamilton County, Ohio, using digital topographic data: dependence of topographic expression of sinkholes on scale, contour interval and slope. J. Cave Karst Stud. 65, 126–129.

Ballevre, M., Martínez Catalán, J.R., López-Carmona, A., Pitra, P., Abati, J., Díez Fernández, R., Ducassou, C., Arenas, R., Bosse, V., Castiñeiras, P., Fernández-Suárez, J., Gómez Barreiro, J., Paquette, J.-L., Peucat, J.-J., Poujol, M., Ruffet, G., Sánchez Martínez, S., 2014. Correlation of the nappe stack in the Ibero-Armorican arc across the Bay of Biscay: a joint French–Spanish project. In: Schulmann, K., Martınez Catalan, J.R., Lardeaux, J.M., Janousek, V., Oggiano, G. (Eds.), The Variscan Orogeny: Extent, Timescale and the Formation of the European Crust. Geological Society, London, Special Publications 405. pp. 77–113. https://doi.org/10.1144/SP405.13.

Barnett-Moore, N., Hosseinpour, M., Maus, S., 2016. Assessing discrepancies between previous plate kinematic models of Mesozoic Iberia and their constraints. Tectonics 35, 1843–1862. https://doi.org/10.1002/2015TC004019.

Bernard-Griffiths, J., Gruau, G., Cornen, G., Azambre, B., Macé, J., 1997. Continental lithospheric contribution to alkaline magmatism: isotopic (Nd, Sr, Pb) and geochemical (REE) evidence from Serra de Monchique and Mount Ormonde Complexes. J. Petrol. 38, 115–132.

Boillot, G., Féraud, G., Recq, M., Girardeau, J., 1989. Undercrusting by serpentinite beneath rifted margins. Nature 341, 523–525.

Bronner, A., Sauter, D., Manatschal, G., Péron-Pinvidic, G., Munschy, M., 2011. Magmatic breakup as an explanation for magnetic anomalies at magma-poor rifted margins. Nat. Geosci. 4, 549–553.

Calais, E., D'Oreye, N., Albaric, J., Deschamps, A., Delvaux, D., Déverchère, J., Ebinger, C., Ferdinand, R.W., Kervyn, F., Macheyeki, A.S., Oyen, A., Perrot, J., Saria, E., Smets, B., Stamps, D.S., Wauthier, C., 2008. Strain accommodation by dyking in a youthful continental rift, East Africa. Nature 456, 783–787.

Choi, J.H., Edwards, P., Ko, K., Kim, Y.S., 2016. Definition and classification of fault damage zones: a review and a new methodological approach. Earth Sci. Rev. 152, 70–87.

Clague, D.A., Reynolds, J.R., Davis, A.S., 2000. Near-ridge seamounts chains in the North-Eastern Pacific Ocean. J. Geophys. Res. 105 (B7), P16541–P16561.

Davis, A.S., Gray, L.B., Clague, D.A., Hein, J.R., 2002. The Line Islands revisited: new $^{40}Ar/^{39}Ar$ geochronologic evidence for episodes of volcanism due to lithospheric extension. Geochem. Geophys. Geosyst.(3). https://doi.org/10.1029/2001GC000190.

D'Oriano, F., Angeletti, L., Capotondi, L., Laurenzi, M.A., López Correa, M., Taviani, M., Torelli, L., Trua, T., Vigliotti, L., Zitellin, N., 2010. Coral Patch and Ormonde seamounts as a product of the Madeira hotspot, Eastern Atlantic Ocean. Terra Nova 22, 494–500.

Féraud, G., Bonin, J., Olivet, J.-L., Auzende, J.-M., Bougault, H., 1977. Sur quelques datations du volcanisme alcalin de la ligne Açores-Gibraltar et leur contexte géodynamique. CR Acad. Sci. Paris 285, 1203–1206.

Féraud, G., Schmincke, H.U., Lietz, J., Gastaud, J., Pritchard, G., Bleil, U., 1981. New K-Ar ages, chemical analyses and magnetic data of rocks from the islands of Santa Maria (Azores), Porto Santo and Madeira (Madeira Archipelago) 636 and Gran Canaria (Canary Islands). Bull. Volcanol. 44, 359–375.

Féraud, G., Gastaud, J., Auzende, J.-M., Olivet, J.-L., Cornen, G., 1982. $^{40}Ar/^{39}Ar$ ages for the alkaline volcanism and basement of Gorringe Bank, North Atlantic Ocean. Earth Planet. Sci. Lett. 57, 211–226.

Féraud, G., York, D., Mével, C., Cornen, G., Hall, C.M., Auzende, J.-M., 1986. Additional ^{40}Ar-^{39}Ar dating of the basement and the alkaline volcanism of Gorringe Bank (Atlantic Ocean). Earth Planet. Sci. Lett. 79, 255–269. https://doi.org/10.1016/0012-821X(86)90184-6.

Féraud, G., Girardeau, J., Beslier, M.-O., Boillot, G., 1988. Datation $^{40}Ar/^{39}Ar$ de la mise en place des peridotites bordant la marge de la Galice (Espagne). CR Acad. Sci. Paris 307, 49–55.

Frizon De Lamotte, D., Fourdan, B., Leleu, S., Leparmentier, F., de Clarens, P., 2015. Style of rifting and the stages of Pangea breakup. Tectonics 34, 1009–1029.

Geldmacher, J., Van der Bogaard, P., Hoernle, K., Schmincke, H.-U., 2000. The $^{40}Ar/^{39}Ar$ age dating of the Madeira Archipelago and hotspot track (eastern North Atlantic). Geochem. Geophys. Geosyst. 1. https://doi.org/10.1029/1999GC000018.

Geldmacher, J., Hoernle, K., Van der Bogaard, P., Zankl, G., Garbe-Schönberg, D., 2001. Earlier history of the ≥70 Ma old Canary hotspot based on the temporal and geochemical evolution of the Selvagen Archipelago and neighboring seamounts in the eastern North Atlantic. J. Volcanol. Geotherm. Res. 111, 55–87.

Geldmacher, J., Hoernle, K., Van den Bogaard, P., Duggen, S., Werner, R., 2005. New $^{40}Ar/^{39}Ar$ age geochemical seamounts Canary and Madeira volcanic provinces: support for the mantle plume hypothesis. Earth Planet. Sci. Lett. 237, 85–101.

Geldmacher, J., Hoernle, K., Klügel, A., Van den Bogaard, P., Wombacher, F., Berning, B., 2006. Origin and geochemical evolution of the Tore-Madeira Rise (eastern North Atlantic). J. Geophys. Res. B09206. https://doi.org/10.1029/2005JB003931.

Geldmacher, J., Hoernle, K., Klügel, A., Van der Bogaard, P., Bindeman, I., 2008. Geochemistry of a new enriched mantle type locality in the northern hemisphere: Implications for the origin of the EM-I source. Earth Planet. Sci. Lett. 265, 167–182.

Grange, M., Scharer, U., Merle, R., Girardeau, J., Cornen, G., 2010. Plume–Lithosphere Interaction during Migration of Cretaceous Alkaline Magmatism in SW Portugal: evidence from U–Pb Ages and Pb–Sr–Hf Isotopes. J. Petrol. 51, 1143–1170.

Gudmundsson, A., Brenner, S.L., 2001. How hydrofractures become arrested. Terra Nova 13, 456–462.

Gudmundsson, A., Simmenes, T.H., Larsen, B., Philipp, S.L., 2010. Effects of internal structure and local stresses on fracture propagation, deflection, and arrest in fault zones. J. Struct. Geol. 32, 1643–1655.

Gudmundsson, A., Lecoeur, N., Mohajeri, N., Thordarson, T., 2014. Dike emplacement at Bardarbunga, Iceland, induces unusual stress changes, caldera deformation, and earthquakes. Bull. Volcanol. 76, 869.

Ishii, E., 2016. Far-field stress dependency of the failure mode of damage-zone fractures in fault zones: results from laboratory tests and field observations of siliceous mudstone. J. Geophys. Res. 121, 70–91.

Jagoutz, O., Müntener, O., Manatschal, G., Rubatto, D., Péron-Pinvidic, G., Turrin, B.D., Villa, I.M., 2007. The rift-to-drift transition in the North Atlantic: a stuttering start of the MORB machine? Geology 35, 1087–1090.

Jiménez-Munt, I., Fernandez, M., Torne, M., Bird, P., 2001. The transition from linear to diffuse plate boundary in the Azores-Gibraltar region: results from a thin-sheet model. Earth Planet. Sci. Lett. 192, 175–189.

Klitgord, K.D., Schouten, H., 1986. Plate kinematics of the central Atlantic. In: Vogt, P.R., Tucholke, B.E. (Eds.), The Western Atlantic Region. Geological Society of America, geology of North America, Boulder, Colorado, pp. 351–378.

Kneller, E.A., Johnson, C.A., Karner, G.D., Einhorn, J., Queffelec, T.A., 2012. Inverse methods for modeling non-rigid plate kinematics: application to mesozoic plate reconstructions of the Central Atlantic. Comput. Geosci. 49, 217–230.

Marine Information Service, 2016. EMODnet Digital Bathymetry (DTM). Marine Information Service. https://doi.org/10.12770/c7b53704-999d-4721-b1a3-04ec60c87238.

Martínez-Loriente, S., Sallarès, V., Gràcia, E., Bartolome, R., Dañobeitia, J.J., Zitellini, N., 2014. Seismic and gravity constraints on the nature of the basement in the Africa-Eurasia plate boundary: New insights for the geodynamic evolution of the SW Iberian margin. J. Geophys. Res. Solid Earth 119, 127–149. https://doi.org/10.1002/2013JB010476.

Matthews, K.J., Seton, M., Muller, R.D., 2011. A global-scale plate reorganization event at 105–100 Ma. Earth Planet. Sci. Lett. 355–356, 283–298.

Merle, R., Caroff, M., Girardeau, J., Cotten, J., Guivel, C., 2005. Segregation vesicles, cylinders, and sheets in vapor-differentiated pillow lavas: examples from Tore-Madeira rise and Chile Triple Junction. J. Volcanol. Geotherm. Res. 141, 109–122.

Merle, R., Scharer, U., Girardeau, J., Cornen, G., 2006. Cretaceous seamounts along the ocean-continent of Iberian margin: U-Pb ages and Sr-Pb-Hf isotopes. Geochim. Cosmochim. Acta 70, 4950–4976.

Merle, R., Jourdan, F., Marzoli, A., Renne, P.R., Grange, M., Girardeau, J., 2009. Evidence of multi-phase Cretaceous to Quaternary alkaline magmatism on Tore-Madeira rise and neighbouring seamounts from $^{40}Ar/^{39}Ar$ ages. J. Geol. Soc. Lond. 166, 879–894.

Merle, R., Jourdan, F., Girardeau, J., 2018. Geochronology of the Tore-Madeira rise seamounts and surrounding areas: a review. Aust. J. Earth Sci. 65, 591–605.

Miranda, R., Valadares, V., Terrinha, P., Mata, J., do Rosario Azevedo, M., Gaspara, M., Kullberg, J.C., Ribeiro, C., 2009. Age constraints on the Late Cretaceous alkaline magmatism on the West Iberian Margin. Cretac. Res. 30, 575–586.

Mitchell, N.C., Masson, D.G., Watts, A.B., Gee, M.J.R., Urgeles, R., 2002. The morphology of the submarine flanks of volcanic ocean islands. A comparative study of the Canary and Hawaiian hotspot islands. J. Volcanol. Geotherm. Res. 115, 83–107.

Natland, J., Winterer, E.L., 2005. Fissure control on volcanic action in the Pacific. p. 687–710 in Plumes, Plates and Paradigms. In: Foulger, G.R., Natland, J., Presnall, D., Anderson, D.L. (Eds.), Geological Society of America. CO, Boulder.

Neres, M., Bouchez, J.L., Terrinha, P., Font, E., Moreira, M., Miranda, R., Launeau, P., Carvallo, C., 2014. Magnetic fabric in a Cretaceous sill (Foz da Fonte, Portugal): flow model and implications for regional magmatism. Geophys. J. Int. 199, 78–101.

Nirrengarten, M., Manatschal, G., Tugend, J., Kusznir, N.J., Sauter, D., 2017. Nature and origin of the J-magnetic anomaly offshore Iberia-Newfoundland: Implications for plate reconstructions. Terra Nova 29, 20–28.

Nirrengarten, M., Manatschal, G., Tugend, J., Kusznir, N., Sauter, D., 2018. Kinematic evolution of the southern North Atlantic: Implications for the formation of hyper-extended rift systems. Tectonics 37. https://doi.org/10.1002/2017TC004495.

O'Connor, J.M., Jokat, W., 2015. Age distribution of Ocean Drill sites across the Central Walvis Ridge indicates plate boundary control of plume volcanism in the South Atlantic. Earth Planet. Sci. Lett. 424, 179–190.

Paduan, J.B., Clague, D.A., Davis, A.S., 2009. Evidence that three seamounts off southern California were ancient islands. Mar. Geol. 265, 146–156.

Peacock, D.C.P., Dimmen, V., Rotevatn, A., Sanderson, D.J., 2017. A broader classification of damage zones. J. Struct. Geol. 102, 179–192.

Peirce, C., Barton, P.J., 1991. Crustal structure of the Tore-Madeira Rise, Eastern North Atlantic-results of a DOBS wide-angle and normal incidence seismic experiment in the Josephine Seamount region. Geophys. J. Int. 106, 357–378.

Pereira, R., Alves, T.M., 2011. Margin segmentation prior to continental break-up: a seismic-stratigraphic record of multiphased rifting in the North Atlantic. Tectonophysics 505, 17–34.

Pereira, R., Alves, T.M., 2012. Tectono-stratigraphic signature of multiphased rifting on divergent margins (deep-offshore Southwest Iberia, North Atlantic). Tectonics 31,

TC4001. https://doi.org/10.1029/2011TC003001.
Pereira, R., Alves, T.M., Mata, J., 2016. Alternating crustal architecture in West Iberia: a review of its significance in the context of NE Atlantic rifting. J. Geol. Soc. 174, 522–540.
Péron-Pinvidic, G., Manatschal, G., 2009. The final rifting evolution at deep magma-poor passive margins from Iberia-Newfoundland: a new point of view. Int. J. Earth Sci. 98, 1581–1597.
Ramalho, R.S., Quartau, R., Trenhaile, A.S., Mitchell, N.C., Woodrooffe, C.D., Avila, S.P., 2013. Coastal evolution on volcanic oceanic islands: a complex interplay between volcanism, erosion, sedimentation, sea-level change and biogenic production. Earth Sci. Rev. 127, 140–170.
Ramos, A., Fernández, O., Torne, M., Sánchez de la Muela, A., Muñoz, J.A., Terrinha, P., Manatschal, G., Salas, M.C., 2017. Crustal structure of the SW Iberian passive margin: the westernmost remnant of the Ligurian Tethys? Tectonics. https://doi.org/10.1016/j.tecto.2017.03.012.
Reynolds, P., Holford, S., Schofield, N., Ross, A., 2018. The importance of subsurface lithology in controlling magma storage vs. eruption: an example from offshore southern Australia. J. Geol. Soc. https://doi.org/10.1144/jgs2017-109.
Ruch, J., Vezzoli, L., De Rosa, R., Di Lorenzo, R., Acocella, V., 2016. Magmatic control along a strike-slip volcanic arc: the central Aeolian arc (Italy). Tectonics 35. https://doi.org/10.1002/2015TC004060.
Sahabi, M., Aslanian, D., Olivet, J.-L., 2004. A new starting point for the history of the Central Atlantic. C. R. Geosci. 336, 1041–1052.
Sallarès, V., Gailler, A., Gutscher, M.-A., Graindorge, D., Bartolomé, R., Gràcia, E., Zitellini, N., 2011. Seismic evidence for the presence of Jurassic oceanic crust in the central Gulf of Cadiz (SW Iberian margin). Earth Planet. Sci. Lett. 311, 112–123.
Sallarès, V., Martínez-Loriente, S., Prada, M., Gràcia, E., Ranero, C., Gutscher, M.-A., Zitellini, N., 2013. Seismic evidence of exhumed mantle rock basement at the Gorringe Bank and the adjacent Horseshoe and Tagus abyssal plains (SW Iberia). Earth Planet. Sci. Lett. 365, 120–131.
Sauter, D., Ringenbach, J.C., Cannat, M., Maurin, T., Manatschal, G., McDermott, K.G., 2018. Intraplate Deformation of Oceanic Crust in the West Somali Basin: Insights from long-offset reflection seismic data. Tectonics 37, 588–603.
Schärer, U., Girardeau, J., Cornen, G., Boillot, G., 2000. 138–121 Ma asthenospheric magmatism prior to continental break-up in the North Atlantic and geodynamic implications. Earth Planet. Sci. Lett. 181, 555–572.
Schettino, A., Turco, E., 2009. Breakup of Pangaea and plate kinematics of the Central Atlantic and Atlas regions. Geophys. J. Int. 178, 1078–1097.
Seton, M., Whittaker, J.M., Wessel, P., Müller, R.D., DeMets, C., Merkouriev, S., Williams, S.E., 2014. Community infrastructure and repository for marine magnetic identifications. Geochem. Geophys. Geosyst. 15, 1629–1641.
Song, X., Li, C.-F., Yao, Y., Shi, H., 2017. Magmatism in the evolution of the South China Sea: Geophysical characterisation. Mar. Geol. 394, 4–15.
Srivastava, S.P., Sibuet, J.-C., Cande, S., Roest, W.R., Reid, I.D., 2000. Magnetic evidence for slow seafloor spreading during the formation of the Newfoundland and Iberian margins. Earth Planet. Sci. Lett. 182, 61–76.
Tesauro, M., Kaban, M.K., Cloetingh, S.A.P.L., 2009. A new thermal and rheological model of the European lithosphere. Tectonophysics 476, 478–495.
Tibaldi, A., 1995. Morphology of pyroclastic cones and tectonics. J. Geophys. Res. 100 (B12), 24,521–24,535.
Tibaldi, A., 2015. Structure of volcano plumbing systems: a review of multi-parametric effects. J. Volcanol. Geotherm. Res. 298, 85–135.
Trippanera, D., Porreca, M., Ruch, J., Pimentel, A., Acocella, V., Pacheco, J., Salvatore, M., 2014. Relationships between tectonics and magmatism in a transtensive/transform setting: an example from Faial Island (Azores, Portugal). Geol. Soc. Am. 126, 164–181. https://doi.org/10.1130/B30758.1.
Tucholke, B.E., Ludwig, W.J., 1982. Structure and origin of the J Anomaly Ridge, Western North Atlantic Ocean. J. Geophys. Res. 87, 9389–9407.
Tucholke, B.E., Sawyer, D.S., Sibuet, J.C., 2007. Breakup of the Newfoundland Iberia rift. In: Karner, G.D., Manatschal, G., Pinheiro, L.M. (Eds.), Imaging, Mapping and Modelling Continental Lithosphere Extension and Breakup. Geological Society, London, Special Publication 282. pp. 9–46.
Veludo, I., Dias, N.A., Fonseca, P.E., Matias, L., Carriho, F., Haberland, C., Villaseñor, A., 2017. Crustal seismic structure beneath Portugal and southern Galicia (Western Iberia) and the role of Variscan Inheritance. Tectonophysics 717, 645–664.
Vergés, J., Fernàndez, M., Martínez, A., 2002. The Pyrenean orogen: Pre-, syn-, and post-collisional evolution. J. Virtual Explor. 8, 55–74.
Vissers, R.L.M., Meijer, P.T., 2012. Iberian plate kinematics and Alpine collision in the Pyrenees. Earth-Sci. Rev. 114, 61–83.